# Kinetics of Phase Transformation and Cross-sectional TEM Studies of Tungsten Silicide Thin Film

A Thesis Submitted in

Partial Fulfillment of the Requirements

For the Degree of

**Master of Technology**

**By**

**Saswat Bharat**

To the

**DEPARTMENT OF MATERIALS AND METALLURGICAL ENGINEERING**

**INDIAN INSTITUTE OF TECHNOLOGY, KANPUR**

**April, 2003**

# CERTIFICATE

**THIS IS TO CERTIFY THAT THE WORK CONTAINED IN THIS THESIS ENTITLED**

*("KINETICS OF PHASE TRANSFORMATION AND CROSS-SECTIONAL TEM STUDIES OF TUNGSTEN SILICIDE THIN FILM")*

By **Saswat Bharat**, has been carried out under our supervision for the partial fulfilment of his master's degree, and his work has not been submitted elsewhere for any other degree.

Monica Katiyar

**Dr. Monica Katiyar,**
Associate Professor
Dept. of Materials and Metallurgical Engineering,
Indian Institute of Technology, Kanpur.

*Dedicated*

*To*

*My Parents & Guide*

# Acknowledgement

I take this opportunity to express my deep indebtedness to Dr.Monica Katiyar and Dr Deepak Gupta for their valuable guidance and supervision towards the completion of my M.Tech thesis work. Their incessant encouragement and suggestions were invaluable. It was indeed an honour to work under them.

It was great pleasure to be with Mr.Vrijendra Kumar of Phase Stability lab in IIT Kanpur. I would like him for his time-to-time advice and allowing me to use his labrotory facilities. My special thanks to Mr.Gautama for his wholehearted guidance for preparation of Cross-sectional TEM samples during my M.Tech course.

My special thanks to Dr.J Narayan, Chief Engineer in Electrical Department who allowed me to use his four-point probe instrument for my thesis work. I am also grateful to Dr.A.K Naik, Assistant Registrar, IIT Kanpur, Mr.Ambirish Mishra, Mr. Kartik Mohapatra, Mr.Bhupalendra Behera and Mr. Dipti Ranjan Sahoo for their generous support right from beginning of my endeavours in this course. I am also thankful to my lab mates Himanshu, Surendra, Amitesh and Asha for their support and encouragement, which made me belief that there is no limit being helpful.

Finally I gratefully acknowledge my parents, brothers and sister, my beloved uncle and aunt for their continuous support in every step of my life, without which it would have been impossible for me to reach this stage.

# Abstract

Development of sub-micron integrated circuit devices has attracted considerable attention in semiconductor technology in recent years. Various new materials and processes are being developed for the sub-micron devices. In particular, refractory metal silicides have attracted interest because of the possibility of using them as gate and interconnect metallization material. As deposited tungsten silicide films are amorphous and have to be subjected to high temperature anneal to achieve the desired electrical properties. Electrical characterization of $WSi_x$ thin films reveals that the resitivity is affected by the composition-Si/W ratio, crystal structure, grain size, substrate type and post deposition heat treatment. So far, the relationship between structure and electrical property of film is not well understood. Moreover, the kinetics of phase transformation of $WSi_x$ thin film deposited by CVD is not investigated.

We have used CVD deposited $WSi_{2.4}$ films on Si and $SiO_2$ substrate and studied phase transformation kinetics. It is observed that phase transformation occurs from amorphous to tetragonal at 1000°C. Using Avrami model for phase transformation, the growth parameter value 'n' for the first five minutes of annealing for $WSi_{2.4}$/Si and $WSi_{2.4}/SiO_2$/Si is found to be 1.36 and 1.23, respectively. This indicates random nucleation and parabolic growth. Crystallization is assisted by Si diffusion away from the grains. The growth parameter decreases for annealing beyond 5 minutes and is found to be ~0.34 on both substrates, which indicates, zero nucleation rate (early site saturation). The grain growth is controlled by long range diffusion of excess silicon.

We were successful in making cross-sectional TEM samples from $WSi_x$/Si film annealed at 700°C for 30 min. We observed grains of average diameter 80 nm through out the silicide layer. This observation is in agreement with the grain size calculation from the X-ray peak widths and with our kinetic model for phase transformation. From selected area diffraction (SAD) pattern, it was observed that grains are single crystal and the symmetry of pattern is that of a tetragonal crystal. We also observe in the cross-section image that silicon is diffusing to the interface and depositing there, this is consistent with earlier observation of reduction in thickness and Si/W ratio of $WSi_{2.4}$ film.

# CONTENTS

# LIST OF FIGURES

# LIST OF TABLES

# CHAPTER 1

# INTRODUCTION

## 1.1. BACKGROUND

As device dimensions continue to decrease in the drive to ever-increasing levels of integration, severe demands are being made upon interconnection technology and metallization. Some of the materials used for this application are listed below:

i) Al and Al Alloys

ii) Cu

iii) Refractory Metals (W, Mo, Ti, Ta, Co)

iv) Nitrides

v) Silicides ($WSi_2$, $MoSi_2$, $TiSi_2$, $TaSi_2$, $CoSi_2$)

Aluminium used to be the most widely used material for interconnections and metallization layers in VLSI technology during its early years. It has many advantages compared to other materials, like high conductivity, excellent adhesion to Si and $SiO_2$, low resistance of ohmic contacts to p-type and heavily doped n-type Si, easy deposition by evaporation techniques and capability of being readily defined into high resolution patterns.[1] But due to some major disadvantages alternative metallization systems have been suggested These disadvantages are, low melting point of the aluminium-silicon eutectic (577°C), rapid diffusion of aluminium along grain boundaries, open circuit failure under electrical stress because of low activation energy for self diffusion, and corrosion under exposure to moisture or air during operating of devices.[2] To avoid these problems doped polycrystalline silicon (poly-Si) was introduced for MOS (Metal Oxide Semiconductor) and CMOS (Complementary Metal Oxide Semiconductor) integrated circuits, but high resistivity ($10^{-4}\Omega$-cm) of poly –Si resulted in degradation of the speed of circuits due to high R-C delay times.[3,4] Consequently refractory metals such as Mo, Ti, Ta, Co and W replaced doped poly-Si. Tungsten offers many advantages over other refractory metals due to desirable properties like matching thermal coefficient of expansion to silicon, ohmic contact, good adhesion to Si and $SiO_2$, capability of being readily defined into high-resolution pattern, high thermal stability, low resistivity, good

defined into high-resolution pattern, high thermal stability, low resistivity, good resistance to electro-migration and excellent diffusion barrier properties [3]. However, refractory metals can not withstand oxidizing ambient at high temperature, because their oxides are generally volatile, and they can not withstand chemical reagents commonly encountered during fabrication of integrated circuits.[3,5] Refractory metal silicides have been proposed as an alternative to tungsten because of their ability to withstand high temperature processing, chemical treatment and thermal oxidation during integrated circuit fabrication.[5] $WSi_2$, $MoSi_2$, $TiSi_2$, $TaSi_2$ and $CoSi_2$ are in this class of refractory silicides. Among these Silicides $WSi_x$ (x is being used as –deposited films are normally non-stochiometry) with or without underlying poly-Si has been used over the past as contact metallization and interconnection for silicon devices in VLSI circuits, because of the following valuable properties.

i. Low resistivity
ii. Ability to withstand various chemical reagents and oxidizing ambient employed in the fabrication of large scale integrated circuits
iii. Good thermal stability
iv. Capability for fine line definition
v. Excellent diffusion barrier properties along grain boundaries and interfaces
vi. Amenable for self-passivation
vii. Good adhesion to substrate and resistance to thermal and mechanical stresses
viii Resistance to electromigration
ix. Thickness uniformity and step coverage

## 1.2. DEVLOPMENT OF NEW MATERIALS AND PRCOCESSES

Although $WSi_x$ is not a new material for this application, development of new semiconductors and smaller devices requires better understanding of this material. Therefore, the focus of this thesis is tungsten silicide, which has found a number of applications in microelectronics. These include:

i. Initial metallization contact to silicon
ii. Gate electrodes and interconnection line material in MOS, CMOS transistors

iii. Buried metal layers in Bipolar Transistors and in DRAM

iv Reflecting layers in photo diodes

v. Ohmic and Schottky gate contact materials

vi Possible ground plane structure for high frequency r f devices

Next, we briefly review the history of the process development for $WSi_x$ layers.

## 1.3. SILICIDE DEPOSITION TECHNIQUE

Several techniques have been used in the past to obtain thin films of silicides and in this section a brief review has been presented. The common techniques used so far for depositing $WSi_x$ films are as follows:

i. Reacting tungsten metal with silicon at high temperature. [6]

ii. Sputtering from a pressed target made of the silicide. [7]

iii. Co-sputtering from two targets (metal and silicon). [8]

iv. Co-evaporation from two electron beam sources. [9]

v. Chemical vapour deposition. [10]

Reacting tungsten metal with silicon was the first technique used to study film properties of $WSi_2$.[6,16] The experiment showed that silicon can migrate through the metal thin film at temperatures much lower than the eutectic point. But as far as W-Si contacts is concerned, the formation of $WSi_2$ by reaction ($W+2Si \rightarrow WSi_2$) affects the ohmic behaviour of contacts, and imposes temperature and time limitations on device processing steps subsequent to the metallization.

Sputtering from a composite target was the next technique used to study the film properties of $WSi_2$.[3,16] However it was quickly realized that the resulting films had a high level of contaminants such as carbon and oxygen mainly originating in the composite target resulting in degraded performance of the silicides. In addition to this, another major problem was control of the stochiometry in sputtered films

Co-sputtering from two separate targets of the metal and silicon improved the properties of the film.[13,14,16]. However, contaminants are not totally removed. The noble gas used for sputtering is inserted in the film especially at the interface and can affect its properties.[8, 16] In general, step coverage of sputtered films is not as

good as that obtained by CVD. Co evaporation of metal and silicon from two e-beams has been used and has provided very pure films.[7, 15, 16] But the main disadvantage is that step coverage is not good and the manufacturability of the process is poor Another major disadvantage of these two techniques is that the deposited material is not a silicide but an amorphous mixture of metal and silicon.

There are some other techniques that have been tried to deposit thin films of a metal on silicon. They are·

i. Thermal Heating [16]
ii. Laser Irridation [16]
iii Ion Implantation of heavy species [17]

The main drawbacks with these techniques are change of volume and uneven interface of the film [16]

Tom et al demonstrated that CVD technique can lower impurities, smoothen interface, lower stress and improve step coverage [18] They used $SiH_2Cl_2$ (dichlorosilane) and $WF_6$ (tungsten hexafluoride) for the deposition of $WSi_x$ This new technique was reported to be cleaner, because $SiH_2Cl_2$ is less reactive than $SiH_4$ resulting in lower fluorine concentrations in the film.

## 1.4. POST-DEPOSITION PROCESSING

These days, the most common technique for depositing tungsten silicide is chemical vapour deposition, but as-deposited films are amorphous; therefore, post-deposition annealing is done to crystallize the $WSi_x$ in its tetragonal form, which has the lowest resistivity required for our application

### 1.4.1 ANNEALING TECHNIQUE:

Tungsten silicide, which is deposited by CVD technique, is annealed at higher temperature to get the desired properties. It was shown that $WSi_x$ deposited by this technique has low resistivity and low contamination. After deposition, $WSi_x$ films are amorphous in nature, but after annealing at the desired temperature, the phase changes from amorphous to crystalline The resistivity of the film also decreases with respect to the increase in temperature. $WSi_x$ film changes from amorphous to hexagonal at

temperature of ~ 550 $^0$C. At higher temperature anneals it transforms directly into a tetragonal phase. The temperature at which the film changes from hexagonal to tetragonal structure depends on the composition of the film, type of the substrate etc. This tetragonal phase is an important from the device point of view because it has low resistivity, high stability of interface at up to high temperature, low stress in the film and compatibility with silicon processing. After such anneal the films becomes inert towards chemical reagents and oxides, which is employed in polysilicon-gate MOSFET technology.

Tsai et.al [19] first reported $WSi_2$ resistivity as a function of time and temperature for co- evaporated films. He suggested that 30 min at 1000°C is needed to completely convert the amorphous phase into tetragonal. Since that report, this process has become standard anneal process irrespective of the deposition technique used. In this thesis I have studied the annealing behaviour of $WSi_x$ films deposited by chemical vapour deposition, which is the common technique used currently in the industry.

## 1.5 KINETICS OF PHASE TRANSFORMATION

The phase transformation kinetics of $WSi_x$ deposited by CVD has never been studied. Therefore, we are studying the kinetics part, which is very important from the device point of view. From processing point of view, $WSi_x$ film is normally deposited on Si and $SiO_2$ layer. We believe that phase transformation kinetics could be different for Si and $SiO_2$ substrate. Therefore, phase transformation kinetics of tungsten silicide films on Si and $SiO_2$ substrate has been studied.

Nava et al [20] studied kinetics of amorphous to hexagonal and hexagonal to tetragonal transformation in the temperature range of 300-600°C. They studied $WSi_x$ films which were deposited by co-evaporation method. We will compare our results with their work.

The methodology for our study is based on the fact that significant changes in resistivity exit between the transformed and untransformed structures. The change in resistance is utilized to estimate, at constant temperature, the time dependence of the

transformed volume fraction assuming a linear relationship between the instantaneous sheet resistance ρ(t), and volume fraction of the isothermally transformed material, $X_T$ *(t)*.[20]

$$X_T(t) = \frac{(\rho_\alpha - \rho_t)}{(\rho_\alpha - \rho_\beta)} \qquad 1.1$$

where $\rho_\alpha$ and $\rho_\beta$ are sheet resistance of the initial and final phases respectively When the mechanism of this transformation is that of nucleation and growth, the kinetics of phase transformation can be described by "Avrami"relationship as follows:

$$X_T(t) = 1 - \exp[(-K\,t)^n] \qquad 1.2$$

where, $t \rightarrow$ the actual transformation time after the incubation period

K $\rightarrow$ the rate constant

"*n*"$\rightarrow$ the coefficient (parameter) related to the mode of transformation, which can be determined from the plot ln ln $[1/(1-X_T(t))]$ vs. ln t.

Sequences of resistance data were used to study the crystallization process as a function of temperature. The resistance curves were fitted using the above equation to obtained *K* and *n*.

According to this model, there are two cases of solid-state phase transformation

i) Change in composition from parent to product phase,

ii) No change in composition from parent to product phase.

When there is no change in composition growth is controlled by short range movement of atoms across the interface (interface controlled growth) and where there is change in composition growth may be controlled by

i) Grain boundary diffusion (the rate at which solute atoms diffuse to the interface)

ii) Surface diffusion (the rate at which atom move across the interface)

iii) Mixed diffusion (the rate at which both solute and substrate atoms diffuse across the interface)

We expect to see diffusion-controlled transformation in the films as a composition change is required when amorphous $WSi_x$ is transformed to tetragonal $WSi_2$. We will discuss the kinetics part of $WSi_x$ in chapter 5 thoroughly.

## 1.6 OBJECTIVE OF THE THESIS:

Phase transformation kinetics and interface properties are major issues in developing better metallization schemes Surface roughness and presence of voids and stacking faults at the interface are some of the routine problems when annealing $WSi_x$ films Therefore, there are two objectives to this work

i. Understand phase transformation kinetics of CVD deposited $WSi_x$ thin films on Si and $SiO_2$ substrates.
ii. Study the effect of annealing in $WSi_x$/Si interface

In this thesis, following characterization methods are used to study the changes after annealing CVD deposited $WSi_x$ film, resistivity measurement, X-ray diffraction technique, Rutherford back scattering spectroscopy, cross sectional TEM. The data was analysed using Avrami model to understand phase transformation from amorphous to crystalline phase. TEM cross-section was used to study the interface of $WSi_x$/Si after annealing.

## 1.7 THESIS LAYOUT:

The second chapter deals with the literature review, which includes details on CVD, annealing studies, and TEM analysis. The sample preparation, annealing and characterization of the films have been reported in chapter 3. In chapter 4, methods of preparation of TEM samples are described. Experimental results and discussions are analyzed in chapter 5. Kinetics study of tungsten silicide phase transformation is presented in chapter 6. In chapter 7, main conclusions are presented.

# CHAPTER 2

## LITERATURE REVIEW

In this chapter, I present a review of the literature on annealing behaviour of tungsten silicide films to understand the changes in the $WSi_x$ film properties during annealing process. The annealing behaviour of the film is dependent on deposition technique. The three main deposition techniques, discussed here are;

i) RF-sputtering

ii) Co-evaporation

iii) Chemical vapour deposition (CVD)

The discussion is mainly focused on how film resistivity, crystal structure, thickness vary with temperature and time in each case. Since we have studied $WSi_x$ films deposited by CVD, a brief description of the technique is also presented.

### 2.1 RESISTIVITY

In this section I will discuss the changes of resistivity of $WSi_x$ films due to annealing.

#### 2.1.1 RF-SPUTTERING

Mohammadi et.al [9] annealed $WSi_2$ thin films deposited by RF-sputtering from a hot pressed silicide target on Si and $SiO_2$. As-deposited films were amorphous in nature, with an average resistivity of $6\times10^{-4}\Omega$-cm, after annealing at 1000°C for 30 minutes in $N_2$ atmosphere; these films attained an average resistivity of about $4\times10^{-4}\Omega$-cm and $5\times10^{-4}\Omega$-cm. As annealing temperature increases, the resistivity decreases and attains a minimum value of about $10^{-4}\Omega$-cm at 1200°C for 30 minutes anneal. Fig 2.1 shows the change in resistivity of the samples annealed for 30 min at 1200°C. As the annealing temperature increased the resistivity decreased. The resistivity of the $WSi_2$ films deposited on poly-Si was slightly lower than the films deposited on $SiO_2$ as shown in Fig 2.1

### 2.1.2 CO-EVAPORATION

Tungsten silicide deposited by co-evaporation technique on polycrystalline silicon (Poly-Si) is also amorphous in nature and has lower resistivity (15-70 μΩ-cm) as compared to films deposited by RF-sputtered methods.[7,19,20] Fig 2.2 shows the sheet resistance of $WSi_2$ annealed at different temperatures. It shows that the sheet resistance decreases within first 15 minutes at 800°C, 900°C and 1000°C, after which improvement is very slow or even close to saturation. This indicates that sheet resistance or resistivity is more sensitive to temperature. To achieve low resistivity i.e. <5 μΩ-cm high temperature annealing (1000°C) is required. Tsai et al also correlated grain size with the sheet resistance, which will be discussed in the next section. Fig 2.2 also reveals that samples annealed at 800°C and 900°C if reannealed at 1000°C for 37 minutes follow the 1000°C annealing curve as shown by the arrows. Their sheet resistance also reduces to 2.7 μΩ-cm.

### 2.1.3 CHEMICAL VAPOUR DEPOSITION

In current technology, tungsten silicide is mostly deposited by CVD technique. Physical properties of the CVD deposited films are different depending on the precursor gases used, for that reason we discuss the annealing behaviour of films deposited by different precursor gases individually.

#### 2.1.3.1 $SiH_4$+$WF_6$+He

Shioya et. al [21] studied tungsten silicide films deposited by CVD using $SiH_4$, $WF_6$, He gases. The deposition temperature was between 325 and 425°C. Fig 2.3 shows the resistivities of as-deposited and annealed $WSi_x$ (x = 2.2, 2.6 and 3.1) films. The deposited films were annealed at different temperatures for 30 minutes and their resistivity was measured. $WSi_x$ (x = 2.2) film having high concentration of tungsten attained maximum resistivity at around 550°C and then it decreased monotonically. For thicker films (2930Å), the film peeled off after annealing at 325-600°C, which is shown by dotted line in Fig 2.3. The peeling off is due to development of large stress in the film during annealing. For $WSi_x$ (x = 2.6) films of thickness 250Å, the resistivity decreased suddenly when annealing at temperature greater than 450°C, but at temperature 550°C resistivity increased slightly. With further annealing resistivity decreased monotonically and attained lower values as compared to as-deposited one,

but for thicker films i.e. in the range of 600-2240Å, the resistivity was almost same in the temperature range 350-500°C, where as resistivity attained maximum value at around 600°C. $WSi_x$ (x = 3.1) films of thickness 225Å, which has higher concentration of silicon, the resistivity decreased monotonically with increasing annealing temperature, but for film thickness in between 575 and 2350Å, the resistivity attained maximum value. The difference between as-deposited and maximum values was smaller for $WSi_x$ (x = 2.2 and 2.6). For thin films, i.e. 225 to 575Å, having x = 3.1 resistivity started increasing at higher temperatures (>1100°C). The reason behind this is due to reaction of $WSi_{3.1}$ with the substrate $SiO_2$. Oxygen diffuses into the $WSi_{3.1}$ film or tungsten diffuses into the $SiO_2$. These results reveal that $WSi_x$ film has a maximum resistivity value at around 600°C and this effect is more pronounced for thicker and in relatively tungsten rich films such as $WSi_{2.2}$. The maximum resistivity at about 600°C is explained by the crystal structure effect. The phase transformation from amorphous to hexagonal structure occurs at this temperature and hexagonal phase has high resistivity. This will be further discussed in the X-ray diffraction analysis part. The summary of this discussion is that annealing behavior is dependent upon Si/W ratio and film thickness. It is concluded that low Si/W ratio and large thickness film can be crystallized easily.

### 2.1.3.2 $Si_2H_6$+$WF_6$+He

Tungsten silicide films, which were deposited by the chemical vapour deposition method using $WF_6$ and $Si_2H_6$, were studied and compared with tungsten silicide films deposited by $WF_6$ and $SiH_4$ Shioya et al.deposited $WSi_x$ films of thickness around 2000Å on the 1000Å oxidized silicon substrates using $WF_6$+$Si_2H_6$ as precursor gas. [4] The annealing temperature depends on resistivities of the $WSi_x$ film, which is shown in Fig 2.4. The resistivity values have maximum at about 600°C and therefore, it has the same annealing behaviour as $WSi_x$ films deposited by $SiH_4$. The resistivity of $WSi_x$ films using $Si_2H_6$ is larger than that of $WSi_x$ films using $SiH_4$ after annealing at 1000°C at the same deposition temperature. It is concluded from above discussion that difference in results is only due to different Si/W ratio of the films, and not due to the change in the precursor gases.

### 2.1.3.3 $SiH_2Cl_2+WF_6+He$

Tom Wu et. al [18]deposited $WSi_x$ films using $WF_6$ and $SiH_2Cl_2$ gases. Films were deposited on nitride and poly-Si substrates at deposition temperatures ranging from 450-650°C. The composition of $WSi_x$ is a function of deposition temperature. The x-value varies from 2.0-2.8 for temperature range of 450-650°C. The deposited films were annealed (RTA) at 1000°C in $N_2$ gas. The deposition was carried out on ~1000Å silicon nitride over silicon to avoid any silicon diffusion to or from the silicon substrate. The resistivity of $WSi_x$ deposited on nitride substrate ranges from $5.0\times10^{-3}$ Ω-cm to $6.5\times10^{-3}$ Ω-cm, where as $WSi_x$ resistivity on poly silicon is around $4.0\times10^{-3}$ Ω-cm. It can be explained that nitride surface acts as a barrier for diffusion of excess silicon at the interface. But it was found that excess silicon in case of poly-Si, can diffuse easily to the interface. It is concluded that after annealing the resistivity of the films deposited by $SiH_2Cl_2$, is fairly insensitive to the deposition temperature, whereas the resistivity of the film deposited by $SiH_4$ and $Si_2H_6$ is sensitive to deposition temperature. [4]

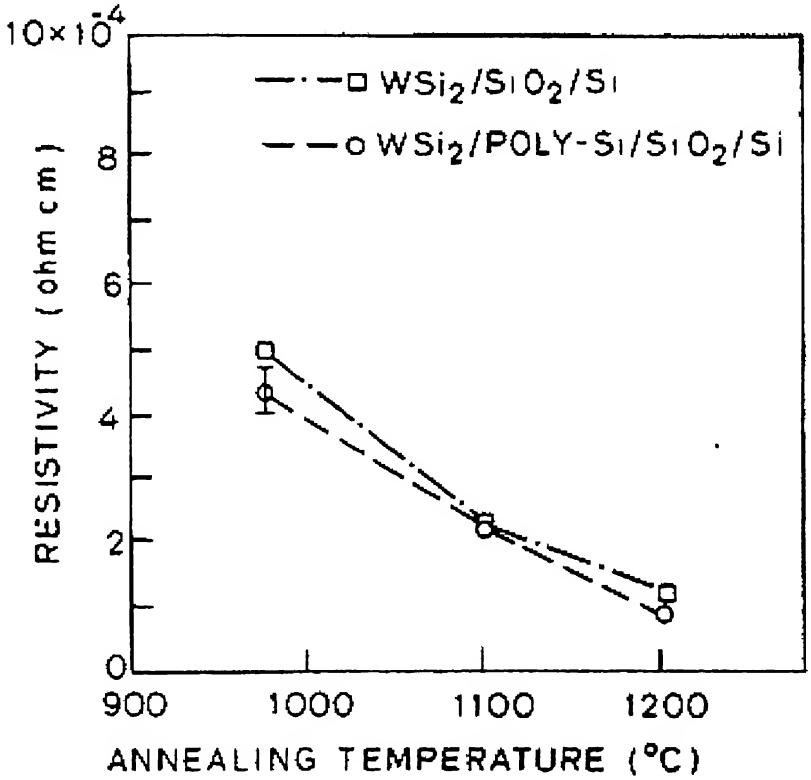


Fig 2.1: Variation of resistivity as a function of annealing temperature for Rf – Sputter deposited $WSi_2$ films. Annealing is done for 30 minute.[9]

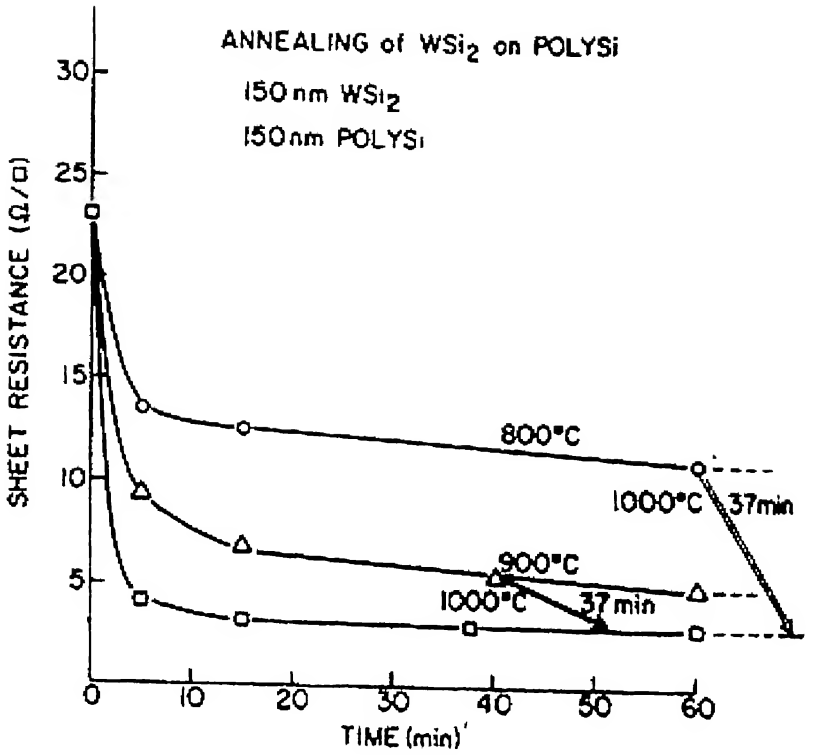


Fig 2.2: Variation of resistivity as a function of annealing temperature for co-evaporated $WSi_2$ films on poly-Si. Annealing is done for 30 minutes. [19]

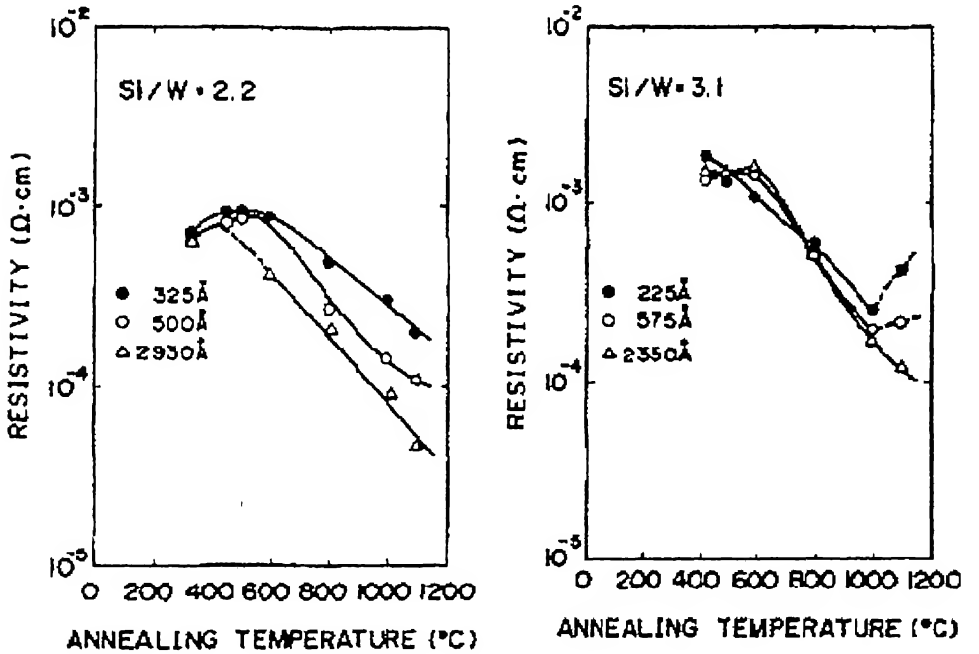

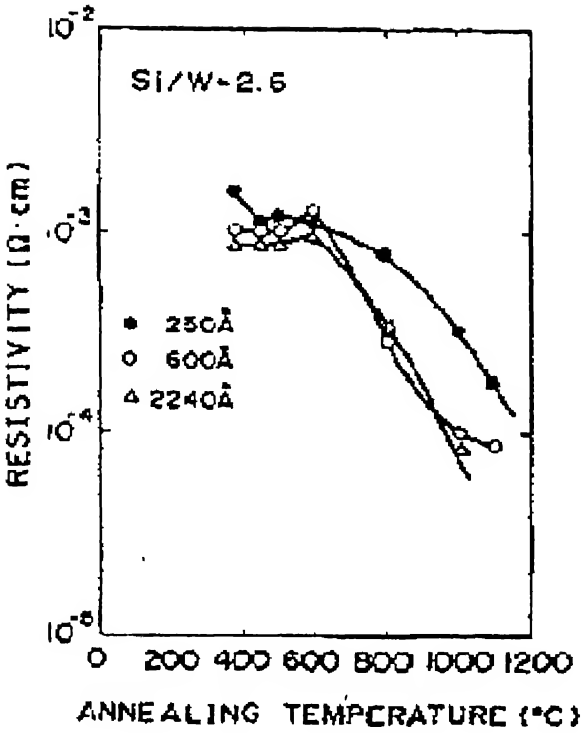


Fig 2.3: Variation of resistivity as a function of annealing temperature for CVD deposited $WSi_x$ (x = 2.2, 2.6, 3.1) films on $SiO_2$ substrates (Annealing is done for 30 minute).[21]

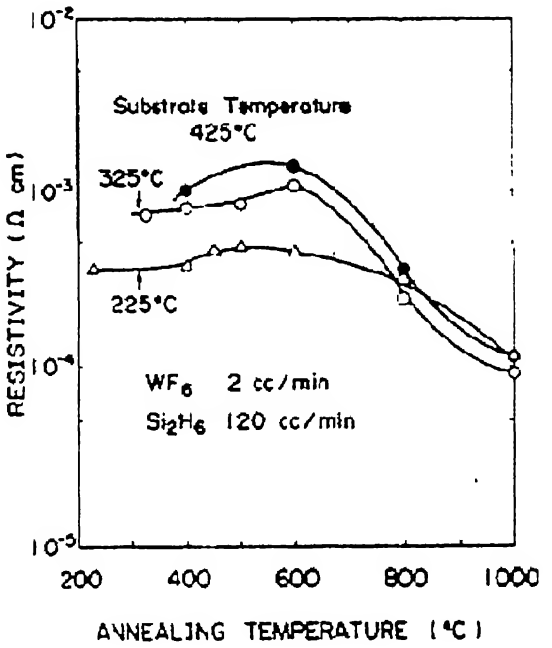


Fig 2.4: Change in resistivity of $WSi_x$ films using $Si_2H_6$ as a function of the substrate temperature. The substrate temperature is 225°C, 325°C, and 425°C.[4]

## 2.2 STRUCTURES, CRYSTALLINITY, GRAIN SIZE

To study the phase transformation in amorphous $WSi_x$, it is important to study crystal structure. X-ray diffraction gives the idea about crystal structure and grain size of the film. In this section I am going to discuss how crystal structure of $WSi_x$ films changes as function of annealing temperature and time.

### 2.2.1 Rf-SPUTTERING

$WSi_x$ films deposited by RF-sputtering are amorphous in nature as observed by X-ray diffraction.[9]. Annealing of $WSi_x$ films at 1000°C makes them polycrystalline with average grain size 500Å. Fig 2.5 shows results of X-ray diffraction of the $WSi_x$ films annealed at 1000°C for 120 minutes. Fig.2.5 shows that the crystallized films do not show any specific orientation of $WSi_2$ [9] As annealing temperature or time increased the intensity of diffraction lines increased but width decreased. This report indicates that degree of crystallization increases with respect to annealing temperature and time.

### 2.2.2 CO-EVAPORATION

Similarly $WSi_x$ films deposited by co-evaporation method are also amorphous in nature. $WSi_x$ films after 60 minutes anneal at 300°C does not show any diffraction pattern. This is for both tungsten rich and Silicon rich films [19]. But after 30 minute anneal at 450°C, the silicon reach film has undergone considerable crystallization where as tungsten reach films reach similar degree of crystallization after anneal at 550°C [7], which is shown in Fig .2.6(a) and 2.6(b). In both cases the poorly defined diffraction peaks are indicative of a rather disorganized crystalline state, a small grain size and high internal micro strains. The film is said to be crystallized between 300°C and 550°C. It is clear from above discussion that the W-rich films appear to be somewhat sluggish and thus require higher temperature than the temperature required for transformations in the stochiometric or Si rich films. The diffraction patterns corresponding to anneals at 650°C and 725°C which is shown in Fig 2.6(a) and 2.6(b) correspond to the well-defined structure of $WSi_2$, tetragonal with a=3.2111Å and c=7.869 Å. Here one can notice that the samples annealed at low temperatures contain extra lines at 13.30, 20.80 and at 23 respectively, which corresponds to

hexagonal structure of $WSi_2$.with a = 4.164 Å and c = 6.414 Å. The estimated temperature for the transition from the hexagonal to the tetragonal structure for silicon rich film is 625°C, where as for W rich film it is estimated as 675°C which is some what higher than the stochiometric films as seen with the evidence presented in Fig 2.6(a) and 2.6(b). The X-ray diffraction patterns obtained after high temperature anneals is quite sharp, corresponding to relatively well order crystalline materials, which can be supplemented by TEM results.[19] The above discussion concludes that W rich films require higher temperature than the silicon rich films for the transition from hexagonal to tetragonal phase.

### 2.2.3 CHEMICAL VAPOR DEPOSITION

#### 2.2.3.1 $SiH_4$+$WF_6$+He

The crystal structures of $WSi_x$ films deposited by CVD methods using $SiH_4$+$WF_6$ precursor gas have also been studied by X-ray diffraction analysis. It is found that mostly as-deposited films are amorphous in nature. Shioya .et al studied the crystal structure of $WSi_x$ of different film thickness as a function of annealing temperature and time. According to them, W/Si = 2.2 film which is tungsten rich is independent of film thickness at 450°C. It was assumed that hexagonal phases appeared at that temperature is independent of film thickness, which is shown in the Fig 2.10 (a). The relative intensities of X-ray diffraction had a maximum value at 500°C and completely disappeared at 800°C [21]. It was observed that $WSi_2$ structure became apparent at low temperatures as films became thicker. A peak for the tetragonal $WSi_2$ appeared at lower temperature of 600°C for a thickness of 600 Å. A peak for the tetragonal $WSi_2$ (112) plane appeared at lower temperature of 600°C for a thickness of 600 Å for silicon rich film having thickness 250 Å, the hexagonal $WSi_2$ did not appear between 500 and 600°C. (Fig 2.10 (b, c)). But for a film thickness of 2240 Å, both hexagonal and tetragonal $WSi_2$ structure began to appear at 450°C shown in Fig 2.10 (d). For richer silicon film $WSi_{3.1}$, even if for thin films of 225 and 575 Å, crystallization occurred above 600°C, but only tetragonal $WSi_2$ structure appeared shown in Fig 2.10 (e). For a thick film of 2350 Å, the hexagonal $WSi_2$ structure began to appear in the deposited state itself. It is concluded from above discussion that, for the relatively tungsten rich films, and even for thicker films, crystallization occurred and the hexagonal $WSi_2$ appeared after low-temperature

annealing. But for the relatively silicon rich films, crystallization occurred only at higher temperature, and even for thicker films, the hexagonal $WSi_2$ structure appeared. So, the main important mechanism is the thicker films can more easily crystallize than the thinner films.[2] Shoiya et.al compared between dependence of X-ray diffraction and annealing temperature on resistivity of annealed CVD $WSi_x$. The resistivity of CVD $WSi_x$ film has a maximum value after about 600°C annealing, because the film has transformed from amorphous state to hexagonal state.

Shoiya et. al also first suggested the relation between the no. of grain boundaries of tetragonal $WSi_2$ in $WSi_{2.4}$ film and the resistivity. He clarified the effect of number of grain boundaries per unit length on the resistivity as shown in Fig 2.10 (f). The grain size was calculated by X-ray diffraction from the Sherror's formulae.

$$\langle D \rangle = \frac{0.9\lambda}{B\cos\theta} \qquad 2.1$$

Where, ⟨D⟩ = Average grain size

$\lambda$ = X-ray wave length ($1.5418A^0$)

B = the width of half amplitude

$\theta$ = Bragg's angle

The Fig.2.10 (f) shows that the resistivity does not decrease monotonically with annealing temperature. These results reveals that for the resistivity to have a maximum value cannot be explained by increase of number of grain boundaries of tetragonal $WSi_2$. It was assumed that the resistivity of the film having a maximum value is related to crystal structure. For $WSi_{2.6}$ film of 600 Å the maximum resistivity is only due to the transition of the amorphous state to the crystalline state. Here it is observed that the tetragonal $WSi_2$ have a small grain size, So It was believed that Si must be segregated in the grain boundaries when the film of $WSi_2$ are crystallized from amorphous state. For tungsten rich films, crystallization is occurred at lower temperatures. This is only due to the segregation of excess silicon in grain boundaries, which is small, and the energy required for crystallization also small. On the other hand $WSi_x$, which is richer in silicon, such as $WSi_{2.6}$ and $WSi_{3.1}$, the increase rate of resistivity induced by crystallization is small because of large amount of excess silicon.

### 2.2.3.2 $Si_2H_6$+$WF_6$+He

The crystal structures of $WSi_x$ films using $Si_2H_6$ were studied by X-ray diffraction analysis. The annealing temperature dependence of X-ray diffraction intensity from various crystal planes of $WSi_{2.6}$ film is indicated in Fig 2.11. The figure shows that the crystallization begins at 400°C; where as the hexagonal structure of $WSi_2$ begin to appear at 550°C.[4] Above 600°C, tetragonal $WSi_2$ becomes the dominant one. This behaviour of crystal structure on annealing temperature is same as that $WSi_x$ films using $WF_6$ and $SiH_4$. The difference between films using $Si_2H_6$ and $SiH_4$ is that X-ray diffraction from the tetragonal $W_5Si_3$ (002) appeared only in the film using $Si_2H_6$ at 800°C and 1000°C. The tetragonal $W_5Si_3$ also appeared in $WSi_{2.2}$ film. A comparison of X-ray diffraction intensities for various compositions of $WSi_x$ films formed by $Si_2H_6$ and $WF_6$ after annealing at 1000°C is given in Table2.2. In the above results it is concluded that for tungsten rich film tetragonal $W_5Si_3$ structure appears easily above 800°C, where as for Si rich films of $WSi_{2.9}$, only tetragonal $WSi_2$ appears. And the diffraction intensity from $WSi_2$ (101) plane becomes the largest. The crystal structure of $WSi_{2.9}$ film is almost same as that of $WSi_{2.2}$ to $WSi_{2.6}$ films using $SiH_4$.

Table 2.2

Comparison of X-ray diffraction intensity for three different $WSi_x$ films after annealing at 1000°C for 30 min in $N_2$ gas

X-Ray diffraction Intensity (arbitrary Units)

| $WSi_x$ | $WSi_2$ T (002) | $WSi_2$ T (101) | $W_5Si_3$ T (002) | $WSi_2$ T (110) | $WSi_2$ T (103) | $WSi_2$ T (112) | $WSi_2$ T (200) |
|---|---|---|---|---|---|---|---|
| $WSi_{2.2}$ | 197 | 231 | 402 | 183 | 153 | 57 | 28 |
| $WSi_{2.6}$ | 328 | 476 | 279 | 432 | 380 | 114 | 48 |
| $WSi_{3.1}$ | 572 | 690 | 0 | 393 | 441 | 177 | 66 |

In summary, I have presented information that indicates that phase transformation kinetics is dependent on the deposition technique Si/W ratio and thickness of the film. Therefore, a standard anneal process determined by the studies on co-evaporated tungsten silicide may not work for films deposited by other techniques. Therefore, there is need to carry out the annealing studies for other cases. Moreover, better understanding of phase transformation kinetics is required to successfully predict the annealing behaviour of various films.

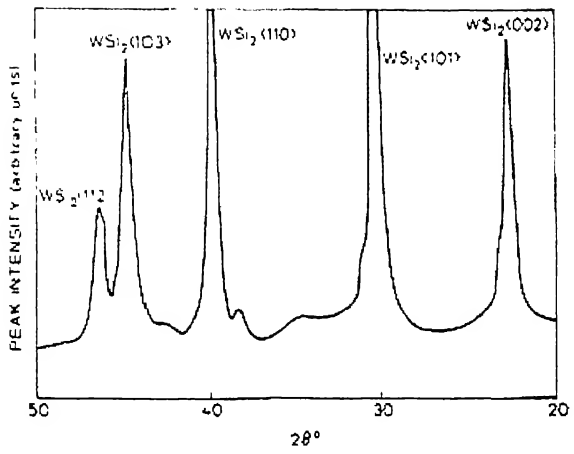


Fig 2.5: X-Ray diffraction pattern of the $WSi_2$ film annealed at 1000°C for 120 minute. Diffraction intensity is plotted as function of twice the angle of incidence 2θ [9]

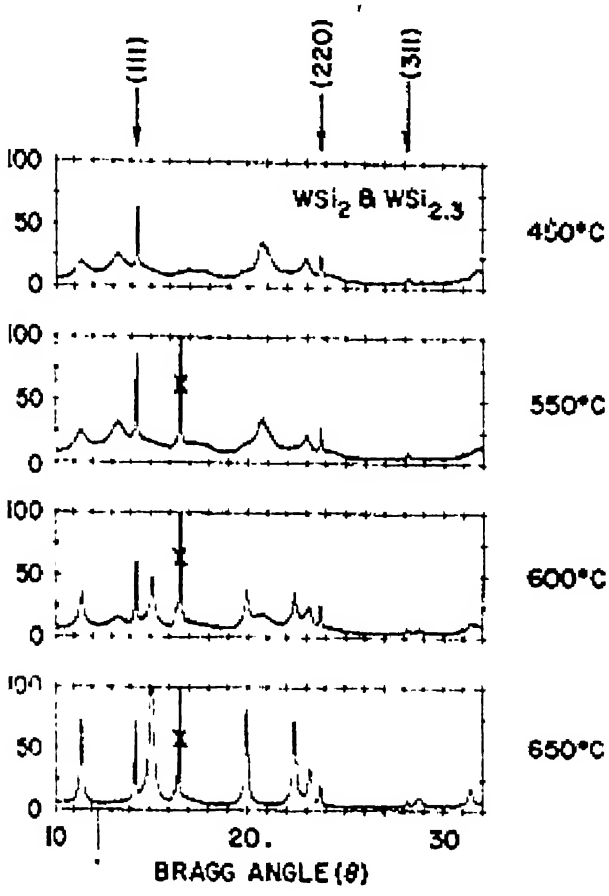


Fig 2.6(a): X-Ray diffraction patterns for $WSi_2$ or $WSi_{2\,3}$ after being anneal at various temperatures for 30 minutes [7]

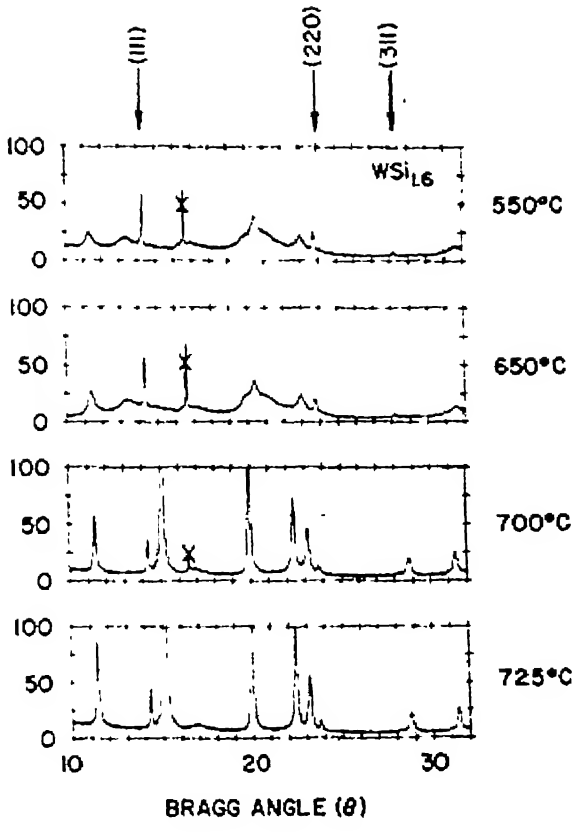


Fig 2.6(b) X-Ray diffraction patterns for $WSi_{1.6}$ after being annealed at various temperatures for 30 minutes [7]

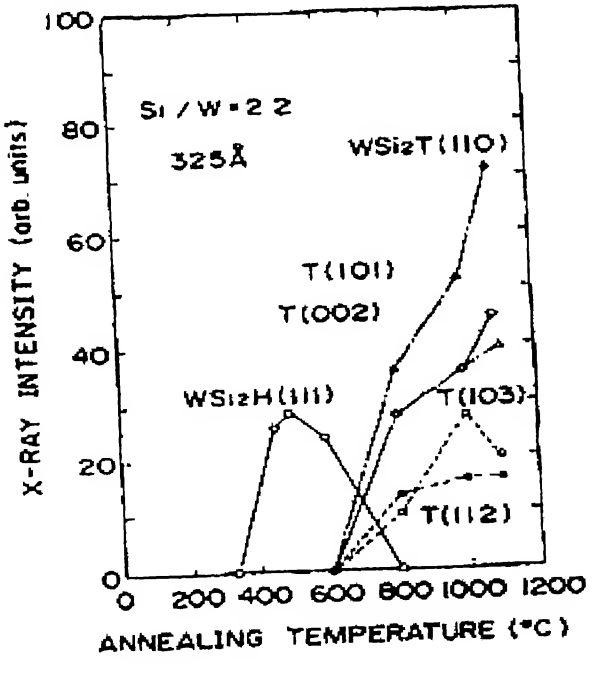


Fig 2.7(a): Relative intensities of X-ray diffraction for $WSi_{2.2}$ films of 325 Å as a function of temperature [21]

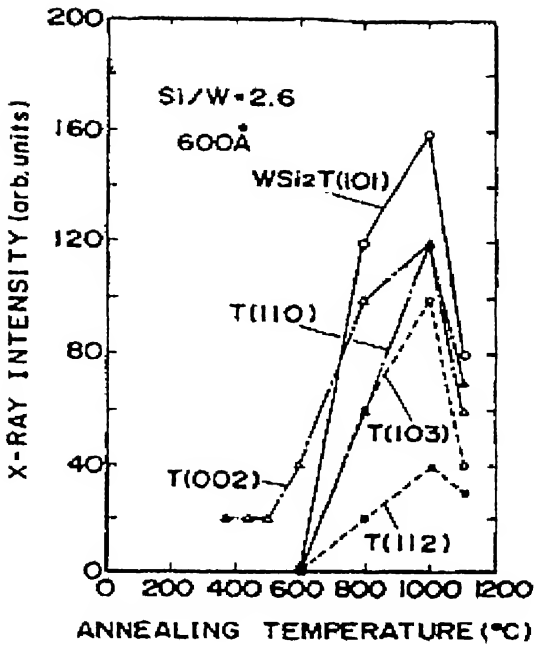


Fig 2.7 (b) Relative intensities of X-ray diffraction for $WSi_{2.6}$ films as function of annealing temperature for 600Å [21]

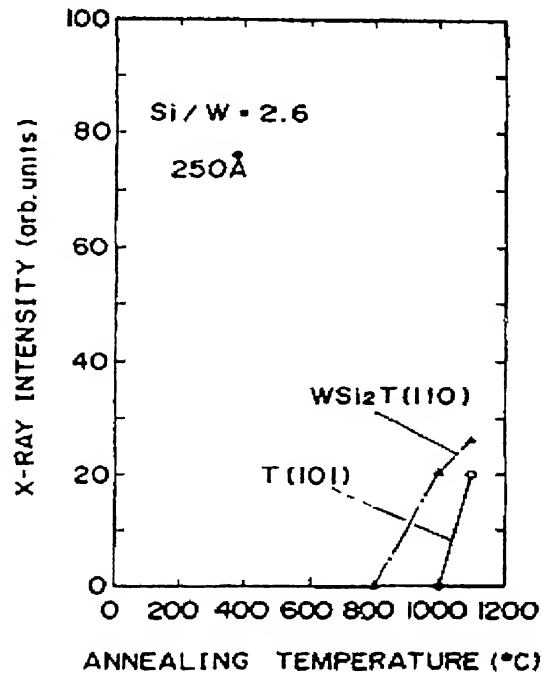


Fig 2.7(c) Relative Intensities of X-ray diffraction for $WSi_{2.6}$ films as a function of temperature for thickness 250Å [21]

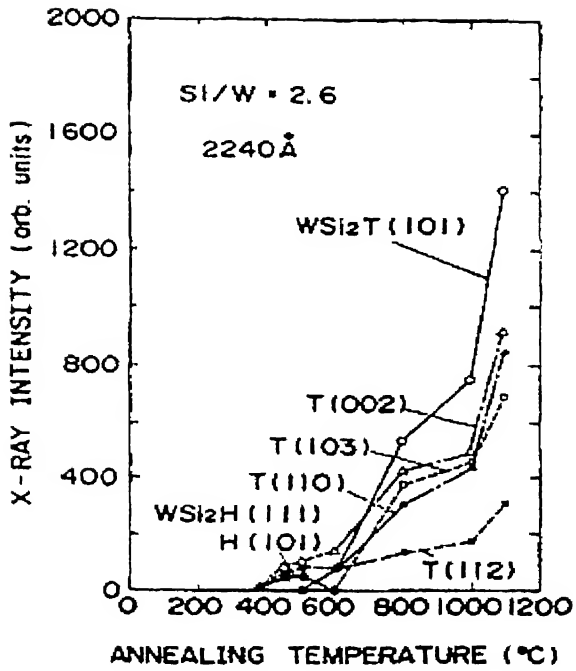


Fig 2.7: (d) Relative Intensities of X-Ray diffraction for $WSi_{2.6}$ films as a function of temperature for thickness 2240Å [21]

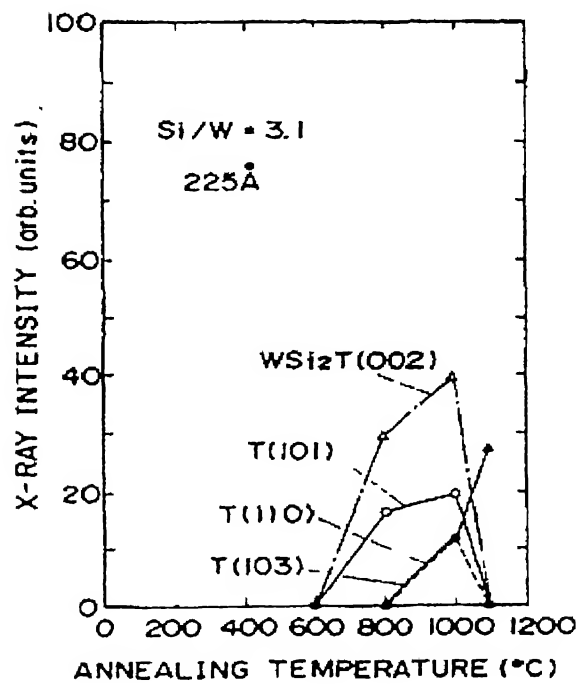


Fig 2.7 (e) Relative Intensities of X-Ray diffraction for $WSi_{3.1}$ films of 225 Å as a function of temperature [21]

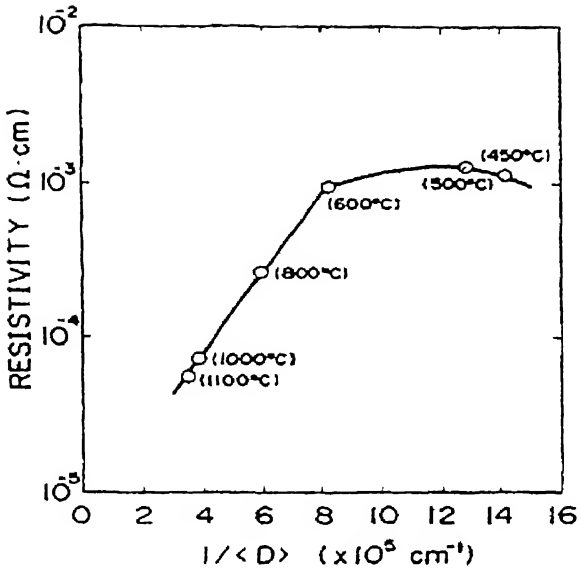


Fig 2.7 (f) Relation between resistivity and number of grain boundaries of tetragonal structure of $WSi_2$ per unit length on $WSi_{2.4}$ film [21]

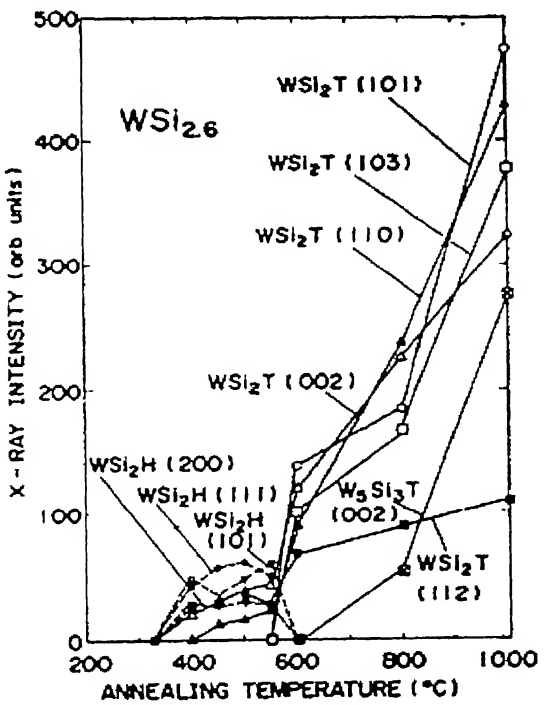


Fig 2.8: Change in X-Ray intensity from various planes of $WSi_{2.6}$ film as a function of annealing temperature. $WSi_{2.6}$ film was deposited at 325°C [4]

## 2.3 TEM ANALYSIS

### 2.3.1 RF -SPUTTERING

TEM studies of the annealed samples of $WSi_2$, which was deposited by rf-sputtering methods and annealed at $1000^0$C for 120 minutes, showed that upon annealing the films became polycrystalline.[9] There is a definite grain structure, with average grain size less than 500Å. From the X-ray diffraction studies it showed that as the annealing temperature or time was increased the intensity of diffraction peaks increased and the width decreased. This indicates that as the temperature or time of annealing is increased the degree of crystallization also increases.

### 2.3.2 CO-EVAPORATION

The sample annealed at 800°C for 30 minutes showed that a large number of small grains formed with a diameter of about, 45nm.(Fig 2.9 (a)) After annealing at 900°C it was found that number of small grains disappeared and average grain size was 50 nm(Fig 2.9 (b)), where as at 1000°C there is formation of fairly equiaxed grains with an average diameter of about 100nm. In Fig 2.9 (c) it can be readily seen that the evolution of the electron diffraction patterns follows quite closely the effects observed in the TEM microstructures.[19]

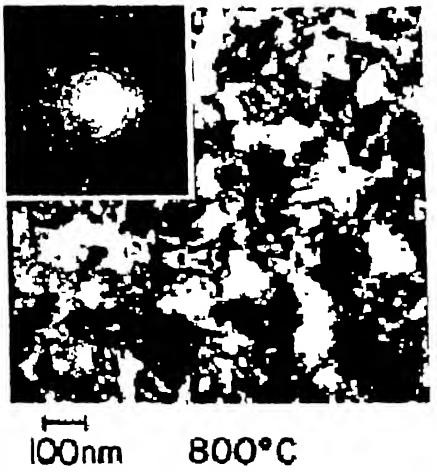


Fig 2.9 (a) TEM Micrographs of $WSi_2$ annealed at 800°C deposited on poly-Si (SAD patterns are also shown)[19]

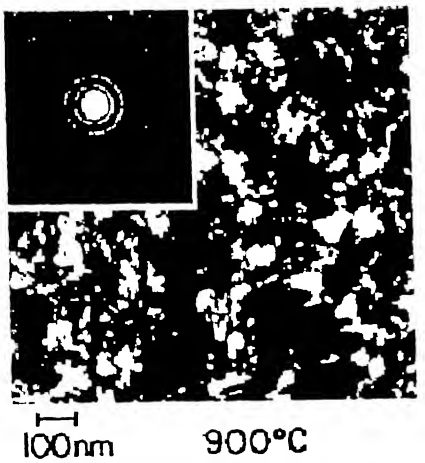


Fig 2.9 (b) TEM Micrographs of $WSi_2$ annealed at 900°C deposited on poly-Si (SAD patterns are also shown)[19]

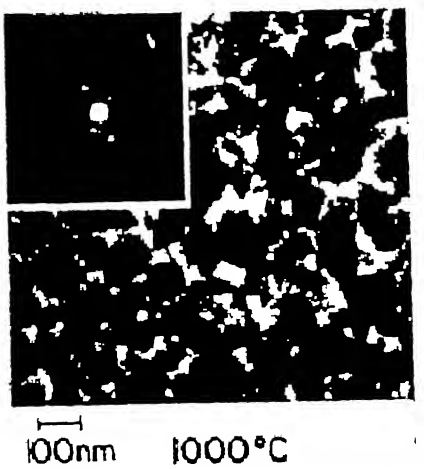


Fig 2.9 (c) TEM Micrographs of $WSi_2$ annealed at 1000°C deposited on poly-Si (SAD patterns are also shown)[19]

### 2.3.3 CHEMICAL VAPOR DEPOSITION

Hara et. al [22] reported cross-sectional TEM of $WSi_x$ film deposited on silicon using dichlorosilane. He first experimented with as-deposited samples, which were deposited at the temperature of 530°C.[22] Fig 2.10(a) shows the cross sectional TEM photograph of $WSi_{2.6}$ and $WSi_x$ ($x<2.0$), which was deposited on Si substrate. The dark area at the interface is a W-rich amorphous layer nucleated by the surface reaction.

But Telford et. al [23] also reported cross sectional TEM of $WSi_x$, which was prepared by $SiH_2Cl_2/WF_6$ chemistry. Fig 2.10(b) shows the cross sectional micrographs of $WSi_x$ films deposited on $SiO_2$ and on poly-Si respectively. The figure reveals in-depth uniformity and the columnar microstructure.

Byun et al [24] correlated resistivity, composition, XRD and cross sectional TEM measurements of in-situ doped poly silicon and dichloride silane $WSi_x$ film. According to them, as deposited polyside has a feathery fine columnar structure.(Fig 2.11(a)) having resistivity about 900 μΩ-cm. After annealing at 900°C for 30 minutes in an $N_2$ ambient, the films converted into polycrystalline grains and resistivity was decreased to 110μΩ-cm. From the view of TEM experiment it was shown in Fig2.10(b) that the diameter of the silicide was approximately less than 100nm. According to RBS study, such a decrease in resistivity is accompanied by the compositional change of the $WSi_x$ film, i.e. x value is going from 2.6 to 2.2 after furnace annealing. This suggests that excessive silicon atoms in the $WSi_x$ ($x>2$) are segregated to the silicide/polysilicon interface during the annealing, probably growing there epitaxially on the existing poly-Si substrate, which is indicated by arrow marks in Fig 2.11(b), where as Fig 2.14(c) shows the plain view of TEM sample. As-deposited samples show polycrystalline hexagonal $WSi_2$ phase, which corresponds to lower temperature structure, with strong (100), (101) reflections. The annealing process resulted in a polymorphic transition to the tetragonal $WSi_2$ phase, a high temperature structure. It appears that film is highly textured in (002) direction.

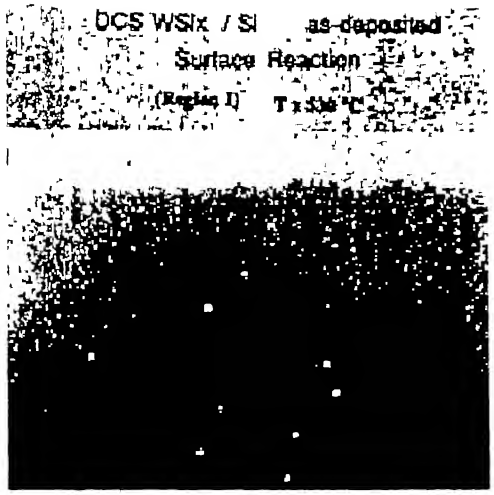


Fig.2.10 (a) Cross sectional transmission electron micrograph of DCS film deposited on Si at temperature of 530°C [22]

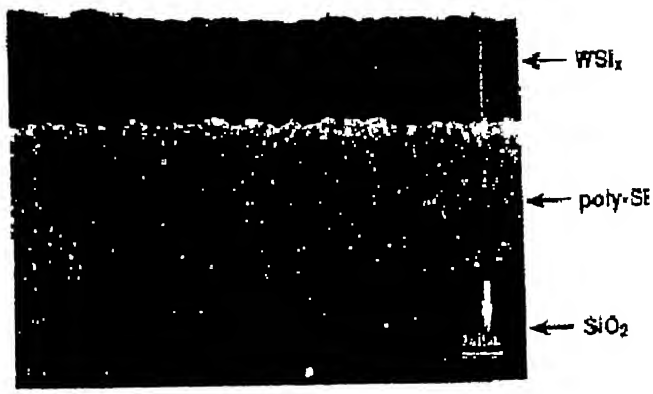


Fig 2.10 (b) Cross-sectional TEM micrographs of DCS $WSi_x$ films deposited on $SiO_2$ and Poly-Si [23]

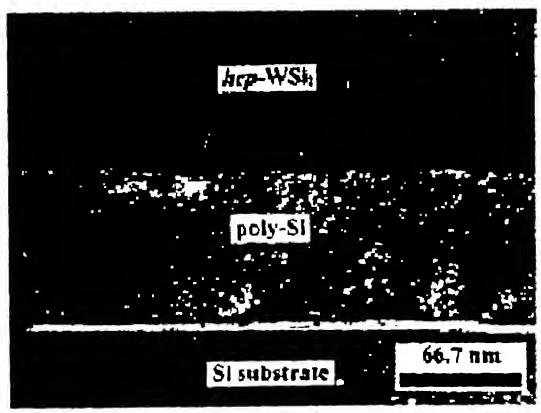


Fig 2.11 (a) Cross sectional view of $WSi_x$ polycide as-deposited on Si substrate [24]

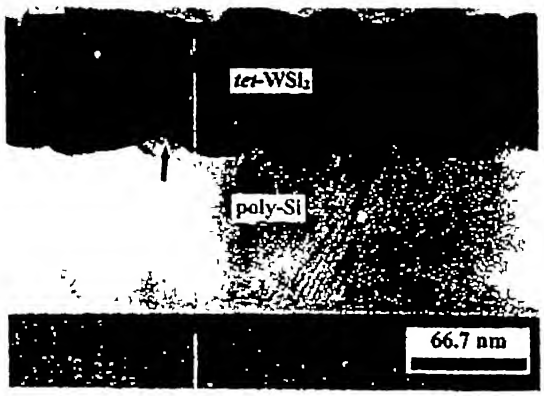


Fig 2.11 (b) Cross sectional view of $WSi_x$ polycide after annealing at 900°C for 30 minutes [24]

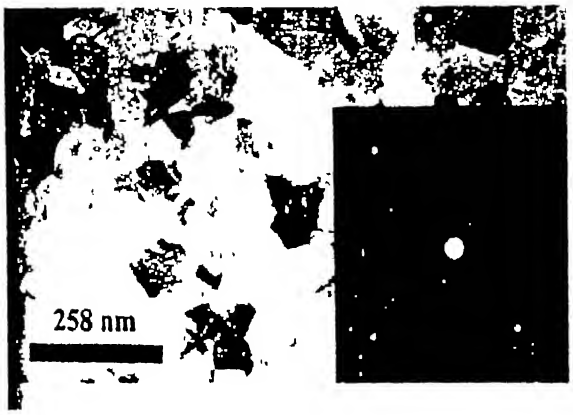


Fig 2.11 (c) Plain view TEM of $WSi_x$ polycide sample annealed at 900°C for 30 minutes [24]

## SUMMARY

From these results it concluded that the (100) grain of hcp-$WSi_2$ might act as a seed for the nucleation of the tet-$WSi_2$ during the polymorphic change. This result reveals that grain growth of the small sized grains during the furnace annealing. On the other hand, an additional furnace annealing did not affect the grain size since the pre existing excess Si atoms would be segregated at the grain boundary of the silicide inhibiting the grain growth during annealing. Therefore, the major factor determining the resistivity is the grain size of the silicide.

# CHAPTER 3

## EXPERIMENTAL DETAILS

This chapter briefly describes the preparation of $WSi_x$ films by CVD and subsequent annealing process. The characterization techniques adopted to study as-deposited and annealed films are also discussed, namely four-point probe method for resistivity, Rutherford backscattering spectroscopy (RBS) for thickness, X-ray diffraction for crystal structure and grain size, transmission electron microscope (TEM) for interface study.

### 3.1 SAMPLE PREPARATION

#### 3.1.1 CVD OF $WSi_X$

Tungsten silicide films were deposited on 8" diameter Si and oxidized Si wafers in an Applied Materials Centura Chamber (at Motorola, Inc.). The deposition temperature was 450°C, and the deposition pressure was 0.6torr.The reactive gases were $SiH_4$ and $WF_6$ and $SiH_4/WF_6$ ratio 235. Samples were cut into several pieces of size (1.5 cm x 0.5 cm) for annealing study. Each sample is encapsulated in an evacuated quartz tube ($10^{-5}$ torr) prior to furnace annealing at 1000°C for time ranging 5minutes to 60 minutes.

#### 3.1.2 ANNEALING PROCESS

It is important from the process point of view that before annealing safer cleaning is done properly. It is essential to remove dust particles and organic impurities, which may be on the sample surface. Otherwise these substances may affect the properties of slicides during the annealing. In my experiments I have adopted following procedure to clean tungsten silicide films deposited on Si and $SiO_2$ substrate.

1. Ultrasonic clean in isopropanol for 5 minutes at 30°C
2. Deionized water wash
3. Blow dried in air

After cleaning each sample is encapsulated in an evacuated quartz tube ($N_2$ ambient at $10^{-5}$ torr) prior to the furnace annealing at temperatures ranging from 500-

1100°C for different times. For annealing at a particular temperature furnace is first stabilized at the annealing temperature before inserting the sample. After annealing sample is allowed to be furnace cooled before taking it out.

## 3.2 CHARACTERIZATION TECHNIQUES

Both as-deposited and annealed samples are characterized by different methods-film resistivity is measured by four-point probe method, film thickness and (Si/W) ratio is measured by Rutherford backscattering spectroscopy (RBS), crystal structure and grain size are measured by X-ray diffractometer. These samples are also examined by transmission electron microscopy (TEM) to study interface structure and morphology.

### 3.2.1 RESISTIVITY MEASUREMENT

Resistivity of various $WSi_x$ films, for both as-deposited and annealed samples is measured by automatic four-point probe method using the following formulae. [25]

$$R_{\text{sheet resistance}} = 4.53\ V/I \qquad 3.1$$

Where, I is current supply through outer probes, V is floating potential drop between two inner probes and 4.53 is the correction factor due to edge effects, thickness effects and probe placements effects. The measurement set-up for four point probe is shown in the Fig.3.1

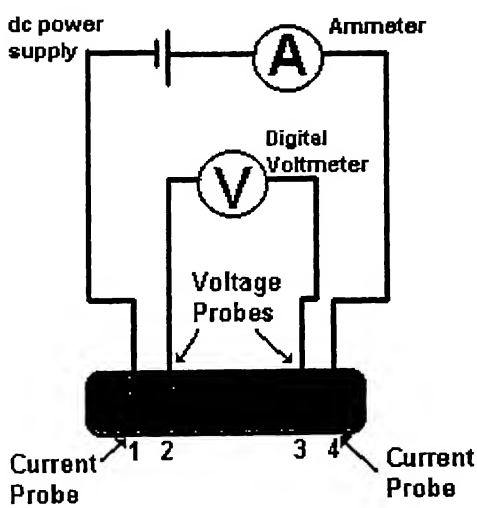


Fig 3.1 Automatic Four-Point arrangement of resistivity measurement

Equation 3.1 is valid when the thickness of the film is vary small compared to the probe spacing. Sheet resistance is measured by applying 4.53ampere current through the outer probes 1 and 4 and measuring the floating potential between the two inner probes 2 and 3. The resistivity is measured by multiplying the measured value of sheet resistance by the average film thickness determined by RBS studies.

### 3.2.2 RUTHORFORD BACKSCATTERING SPECTROSCOPY

Rutherford backscattering spectroscopy (RBS) has found its greatest utility in thin film characterization.[26] RBS is based on back scattering of ions or projectiles incident on a sample. Typically $^4He^{++}$ ions of a high kinetic energy (typically 1-3MeV) are directed at the sample. The incident ions are elastically scattered from the atoms in the sample. The number of scattered ions and their energy is measured. Fig 3.2 and Fig 3.3 show schematics of RBS technique. Ions of mass $M_1$, atomic no $Z_1$ and energy $E_0$ are incident on a target composed of mass $M_2$ and atomic number $Z_2$. Most of incident ions come to rest within the target losing their energy through interactions and some are back scattered from the sample at various angles. For those incident ions scattered by surface atoms, conservation of energy and momentum leads to a relationship between $E_1$ the energy after scattering and $E_0$ the incident energy. The ratio of the projectile energy ($E_1$) after a collision to the projectile energy ($E_0$) before a collision is defined as the kinematic factor. [26,33]

$$K=E_1/E_0 \quad 1-2R\,(1-\cos\theta)/(1+R)^2 \qquad 3.2$$

Where $R=M_1/M_2$ and $\theta$ is the scattering angle. We found out $M_2$ using equation 3.2. Thus, RBS allows determination of masses of the element in the sample, their distribution over a distance from 100Å to a few microns from the surface. In our case, composition (Si/W) ratio and thickness of as-deposited and annealed samples is obtained from RBS. The samples are mounted on a sample holder. This sample holder is placed in an evacuated chamber of RBS setup. $He^+$ ions having 1.23 MeV incident energy, obtained from Van-de-graf accelerator facility setup in IIT Kanpur, are made incident on these samples. These ions after striking the samples are scattered along different direction. Out of these backscattering ions having less energy as compared to incident ions some are collected by a silicon barrier detector, kept at a backscattering angle of 170°. After collecting the RBS spectra, the spectra

was analyzed using the versatile Rump-software package (Do little 1980and 1986). Other condition under which RBS spectra are collected are given in the Table (2)

## Table 3.2

RBS settings used in the experiments

| | |
|---|---|
| Beam parameter | Energy-1.23 Mev (4He+), charge-2 coulomb, current-8Ampere |
| Geometry | Theta (θ)-0.0, Phi (φ)-30.0, Psi-0.0 |
| MCA | Energy conv-2.253, 112.00,First chan-1.0, NPT-512 |
| Detector | FWHM-17.0Kev, Omega (Ω)-2.900 |
| Correction | 1.400 |

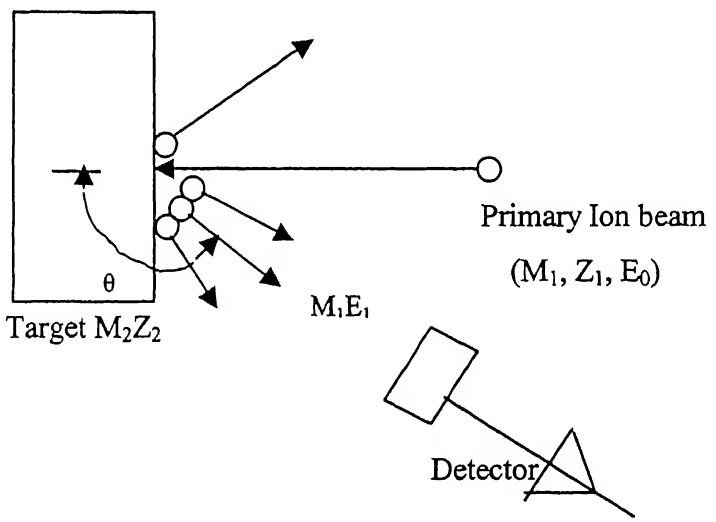


Fig 3.2 Schematic of Rutherford backscattering spectroscopy.

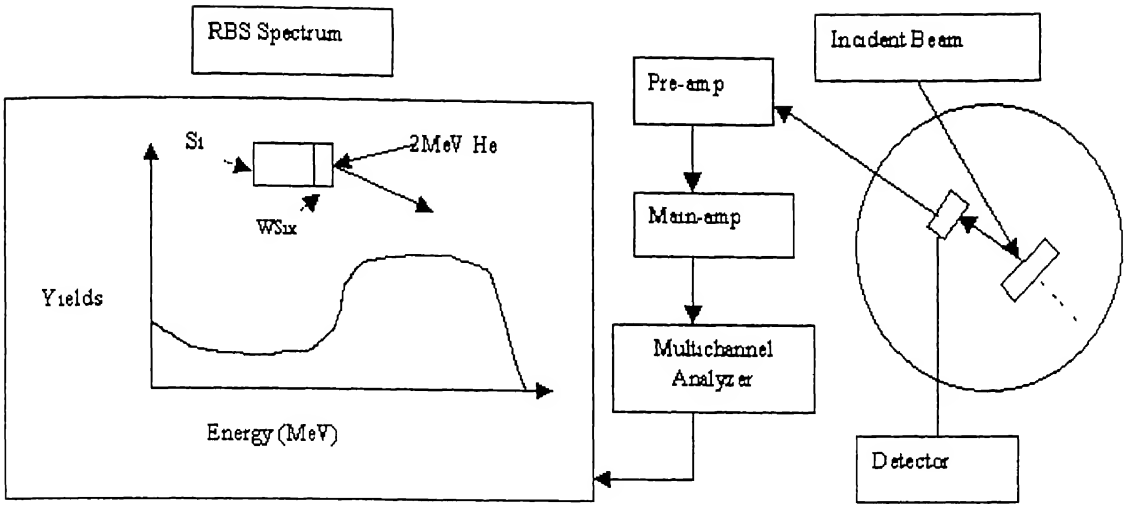


Fig 3.3 Schematic of RBS set-up and data

### 3.2.3 X-RAY DIFFRACTION

The X-Ray diffraction patterns of various $WSi_x$ samples are recorded using a Rich-scifort X-Ray diffract meter (ISO-Debye flex-2002) using $CuK_\alpha$ radiation of wavelength 1.5418Å. The diffracted beam was received by the scintillation counter detector held at an angle 2θ with the transmitted beam. Rotations of the specimen and detector are synchronized to maintain the focusing condition. We recorded the intensity patterns for 2θ values from 20° to 100° at the sweep rate of 3°/min. The X-ray tube is operated at 20 mA and 30 kV.

### 3.2.4 TRANSMISSION ELECTRON MICROSCOPE

We made several cross-sectional TEM samples (XTEM) of $WSi_x$/Si annealed at 700°C for 30 minutes to study the size, shape and arrangement of the grains, as well as their relationship to each other. It was also efficacious for studying the critical interface between $WSi_x$ and silicon

A general description of JEM 200 FX (JEOL) Transmission electron microscope, which is set up in ACMS IIT Kanpur is given below. Details of the sample preparation are given in the next chapter.

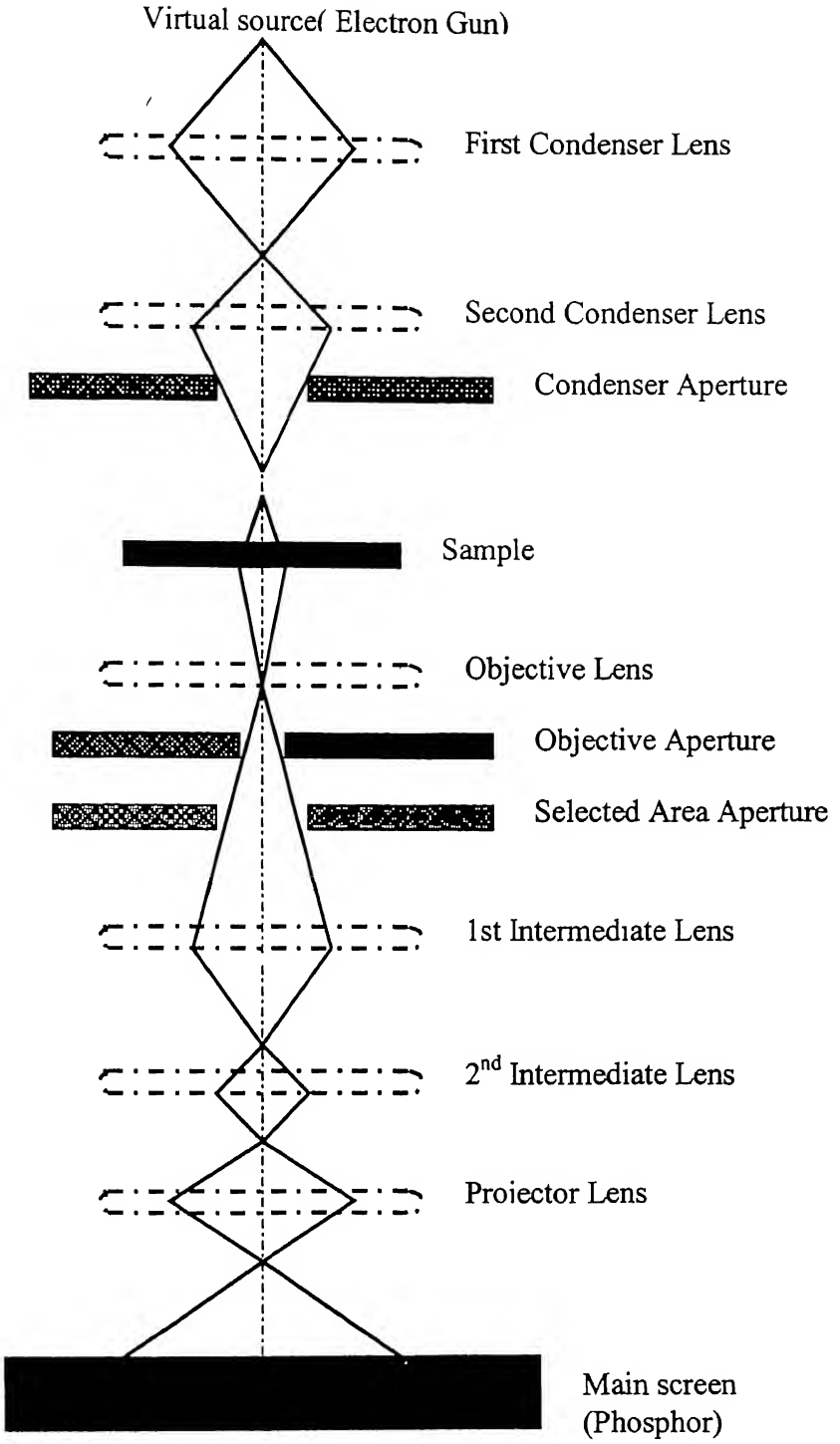


Fig 3.4 JEOL Transmission Electron Microscope

**Description of TEM**

1. The "Virtual Source" at the top represents the electron gun, producing a stream of monochromatic electrons.
2. This stream is focused to a small, thin, coherent beam by the use of condenser lens 1 and 2. The first lens (usually controlled by the "spot size knob") largely determines the "spot size", the general size range of the final spot that strikes the sample. The 2nd lens (usually controlled by the "intensity or brightness knob") actually changes the size of the spot on the sample, changing it from a wide dispersed spot to a pinpoint beam.
3. The beam is restricted by the condenser aperture, knocking out high angle electrons (those far from the optic axis, the dotted line down the center).
4. The beam strikes the specimen and parts of it are transmitted.
5. This transmitted portion is focused by the objective lens into an image.
6. Optical objective and selected area metal apertures can restrict the beam; the objective aperture enhancing contrast by blocking out high angle diffracted electrons, the selected area aperture enabling the user to examine the periodic diffraction of electrons by ordered arrangement of atoms in the sample.
7. The image is passed out the column through the intermediate and projector lens, being enlarged all the way.
8. The image strikes the phosphor image screen and light is generated, allowing the user to see the image. The darker areas of image represent those areas of the sample that is fewer electrons were transmitted through (they are thicker and denser). The lighter areas of image represent those areas of the sample that more electrons were transmitted through (they are thinner or less dense)

# CHAPTER 4

# METHOD OF PREPARATION OF CROSS SECTIONAL TEM SPCIMEN

## 4.1 BASIC CONCEPT

Specimen preparation is an important aspect of the transmission electron microscopy (TEM) analysis of electronic materials. Specimen preparation techniques are very material dependent; therefore, it is important to initially select the technique that is most beneficial for the individual specimen. To study the interface between electronic materials using TEM, it is necessary to prepare cross-sectional specimens. This method of preparation is based on two techniques - dimpling and ion-milling.

## 4.2 SAMPLE PREPARATION

To prepare $WSi_x$ TEM specimen, the desired area of interest is initially obtained from the bulk material. With the help of low speed diamond cut-off saw (Isometric cutter) a series of rectangular wafers having width 3mm are produced which is shown in Fig 4.1(a). These wafers are then cleaned by acetone to remove any contamination of oil or undesired impurities. The wafers are glued into a thin wall brass tube having an outer diameter of 3 mm using F-1 epoxy to prepare sandwiched samples, which is shown in Fig 4.1(b). This epoxy is vacuum compatible and cures at relatively low temperature (60°C), and does not erode as rapidly as other types of epoxy when subjected to energetic ion beams. Before inserting wafers into the brass tube, tube is cleaned properly by $HNO_3$, $H_2SO_4$, and HCl mixture (1:1:1). The holder is then kept vertical for 24 hours by the help of TEM holding plate (Glass plate) Fig 4.1(c) for curing of the epoxy. The cylinder is then cut into 300 μm thickness with the help of low speed diamond cut-off saw shown in Fig 4.1(d). After acquiring a number of disks having 3 mm diameter, all those disks are first washed in soap solution and then in acetone to remove oils and impurities from the disks. After that each disk is submitted to planar polishing, dimpling and ion milling to make thin samples for TEM imaging.

### 4.2.1 POLISHING

Prior to dimpling, it is desirable to reduce the specimen thickness to approximately 100 μm. This is achieved through the use of classic metallographic polishing techniques utilizing a precision, planar specimen grinder. This device allows the rapid removal of large amounts of material in a controlled manner while inducing minimal specimen damage. Polishing is conducted on a wet-type of rotary grinding/polishing wheel. The abrasive size is progressively decreased from 600 grit to 0.5 micron. Final polishing is achieved with Syton cloth pad.

### 4.2.2 DIMPLING

Dimpling is a preparation technique that produces a specimen with a thinned central area and an outer rim of sufficient thickness to permit easy handling.[27] This specimen configuration is achieved by the simultaneous rotation of both the specimen and a grinding wheel containing abrasive slurry (typically diamond) whose axes are orthogonal and intersecting.advacements in process control have greatly increased the capabilities and performance of the dimpling process. After planar polishing, the specimen is demounted, turned over, and reattached to the platen with a low melting point polymer. Ready for the dimpling as shown in Fig 4.2 the platen fits into a magnetic base, coupled to the specimen stage with a rare-earth magnet. To select a specific area on the specimen surface to be dimpled, the magnetic base is easily slid into the appropriate position. This process is conducted while the specimen is being observed through an optical microscope.

The platen contains a glass center portion that permits light to be transmitted from a source located beneath the specimen stage. This feature is particularly important when preparing Si specimens that experience a change in the colour of transmitted light as the specimen thickness is reduced to less than 5 μm .

For results, a progressive sequence of operational parameters is employed. Intially, an aggressive grinding rate of 4.0 μm /minute with a force of 30 grams is used. Three-micron diamond abrasive compound serves as the grinding medium. As the specimen thickness approaches 25 microns, the grinding rate is reduced to 1.0 micron/minute; the grinding force is reduced to 20 grams, and the diamond abrasive is

changed to a one-micron grit size. At a specimen thickness of 10 microns, the grinding rate is reduced to 0.5 microns/minute; the grinding force is reduced to 10 grams and the diamond abrasive is changed to a 0.25-micron grit size. Final polishing is accomplished with a grinding force of 5 grams and a grinding rate of 0.2 micron/minute. Alumina is used as the final abrasive medium. So after dimpling of one side of the sample, the opposite side also dimpled in the same manner.

### 4.2.3 ION MILLING

Ion milling is traditionally the final step of specimen preparation. In this process, charged argon ions are accelerated to the specimen surface by the application of high voltage. The ion impingement upon the specimen surface removes material as a result of momentum transfer. The ion milling system available in ACMS is a versatile, compact, tabletop, precision system designed to consistently produce high quality TEM specimens with large electron transparent areas from a wide range of materials. The system includes two independently adjustable hollow anode discharge ion sources for rapid milling, automatic gas control, a turbo-pumped, vacuum system, a milling angle range of 0 to $45^0$, specimen rotation or rocking, a liquid nitrogen cooled specimen stage, automatic termination, and chemically assisted etching.

## 4.3 PROCEDURE FOR ION MILLING

### 4.3.1 PREPARATION

(a) Open the argon gas and set the precursor to 0.8 $Kg/mm^2$.

(b) Switch on the chiller.

(c) Switch on the power to IBT unit.

(d) Switch on the panel unit.

### 4.3.2 STARTING THE VACUM PUMP

We first switch on rotary pump; diffusion pump is started when vacuum level reaches 500 m.torr.

### 4.3.3 SPECIMEN LOADING

To load the sample press the vent valve and remove the specimen-viewing window. (Making sure that airlock is always in raise position otherwise the whole chamber will open to the atmospheric pressure). Then we cleaned the specimen-viewing window and loaded the sample. After that the airlock in lower position is pressed, so that the pressure reaches $10^{-6}$ in the cold cathode gauge. When the vacuum level reaches $10^{-6}$, the cathode gauge is turned off. Next we depress the vacuum valve intermittently, so that pressure does not go beyond 500 m torr in vacuum gauge. It was done repeatedly until the reading of the vacuum gauge reached 500 m torr.

### 4.3.4 TURN ON THE GUNS

First of all we set the process time (maximum) by pressing the start-stop knob. (made sure air lock is in lower position). Switch on the high voltage and current regulated mode in such a way that high voltage knob should be in fully clockwise position. Set the gun selector switch to white position, switch on the solenoid valve for white gun. Adjust the needle valve to the required voltage, which will be discussed in the next session. The current should be set 0.5 m amp. Set the gun selector switches to red position; switch the solenoid valve for the red gun. Adjust the needle valve to obtain the required voltage. Then switch the gun selector switch to White/red position. Set the gun current to1.0 amp and switch on the specimen voltage.

### 4.3.5 ION SOURCE

A hollow anode discharge (HAD) ion source is used for thinning samples as this type of ion source consume less gas, contain large range of ion beam current density, long component life, and overall ionization efficiency. HAD ion sources provide an ion accelerating voltage range of 0.5 kv to 6.0 kv and an internal plasma current range of 3 mA to 10 mA. Ion beam current densities of up to 400 $\mu amp/cm^2$ are readily produced. Due to the focusing effect of the extraction aperture, 85% of the ion beam is concentrated into a 1.5 mm diameter spot size; therefore,, specimens with

large electron transparent areas are prepared with minimal risk of contamination from either the holding plates or the specimen stage.

Argon gas is introduced through an orifice located in the center of the cathode that is maintained at ground potential. Two independently controlled mass flow controllers automatically regulate gas flow.

Ionization of the argon gas is initiated by the application of a voltage between the anode and cathode. The cathode surface is concave with a precise radius to focus both ions and electrons at the hollow anode discharge portion of the anode where by secondary plasma is formed. It is from this secondary plasma that the positively charged ions are extracted by the application of a negative voltage potential applied to the extraction aperature. This aperture focuses and accelerates the ions to the specimen. For effective ionization, the chamber is evacuated by a turbo molecular vacuum pump that maintains a system vacuum between $1\times10^{-4}$ and $5\times10^{-5}$ torr under normal conditions. Fig 4.3 shows the milling of samples by the impingement of argon gas.

### 4.3.6 SPECIMEN MOUNTING

The specimen is loaded into the milling chamber through an access port containing hinged doors. The chamber is fitted with observation windows and halogen lamp assemblies for specimen viewing. A stereomicroscope is utilized for in-situ specimen monitoring.

### 4.3.7 LIQUID NITROGEN COOLING

Liquid nitrogen prevents the energetic ion beam from thermally altering the material's properties. So, for that reason a liquid nitrogen dewar located within the instrument enclosure is thermally coupled to the specimen stage, which lowers the stage and specimen temperature during milling.

## 4.4. ION MILLING RESULTS

In this method the rate of removal of material is about 1mm/hr. Angle of incidence of laser beam w.r.t specimen was 13 to $30^0$ for both sides of the sample.

After milling about 40 hours I got a large electron transparent area with a uniform thickness, which was used to detect the interface of the film in TEM. Fig 4.4 and Fig 4.5 shows the interface of $WSi_x$ disk and electron transparent area for TEM study after milling. I prepared six sample and was able successfully see the interface in two of them. From my experience, it seems that ion milling time can be considerably reduced if the sample are well thinned in the dimpling m/c. Another important factor is that, as samples become very thin, so one should be very careful in handling the specimen.

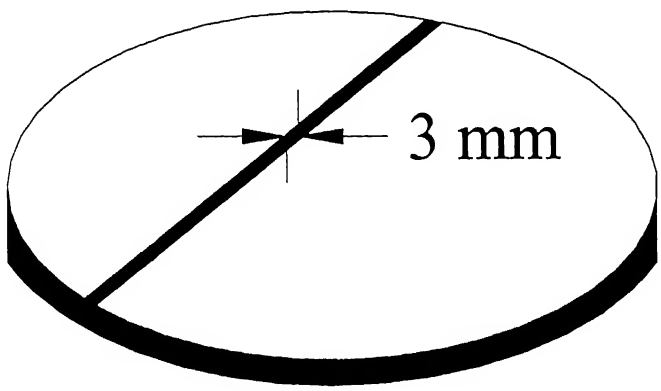


Fig 4.1 Rectangular wafers of width 3mm cut from the parent substrate

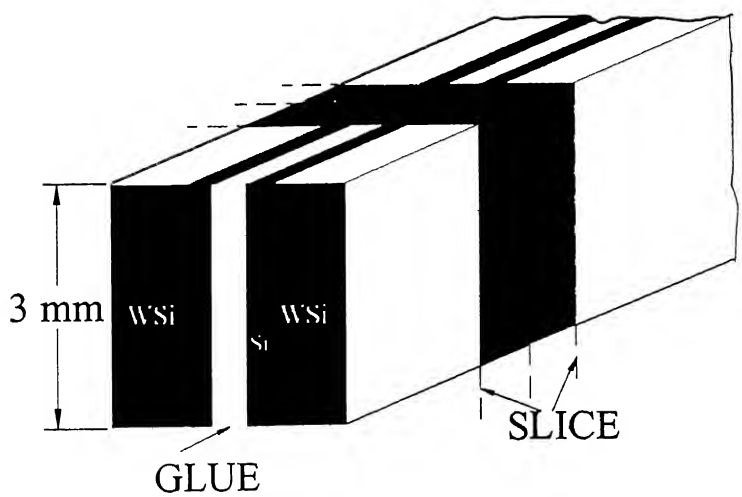


Fig 4.2(a) Picture of Sandwiched samples in TEM Holder

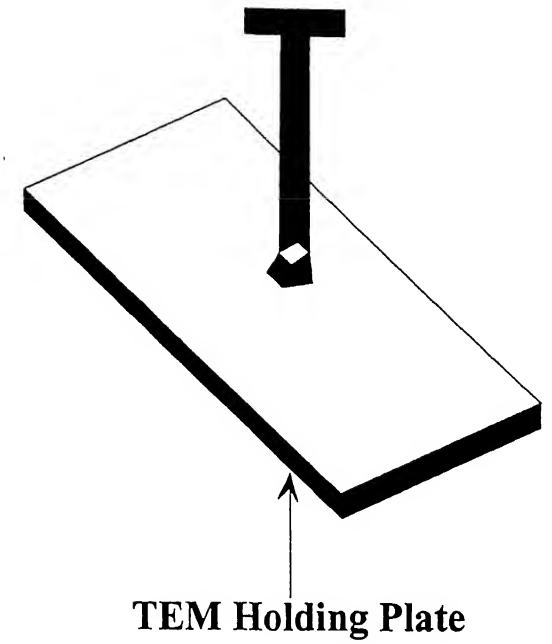


Fig 4.2 (b) TEM Holding plate supports TEM specimen Holder.

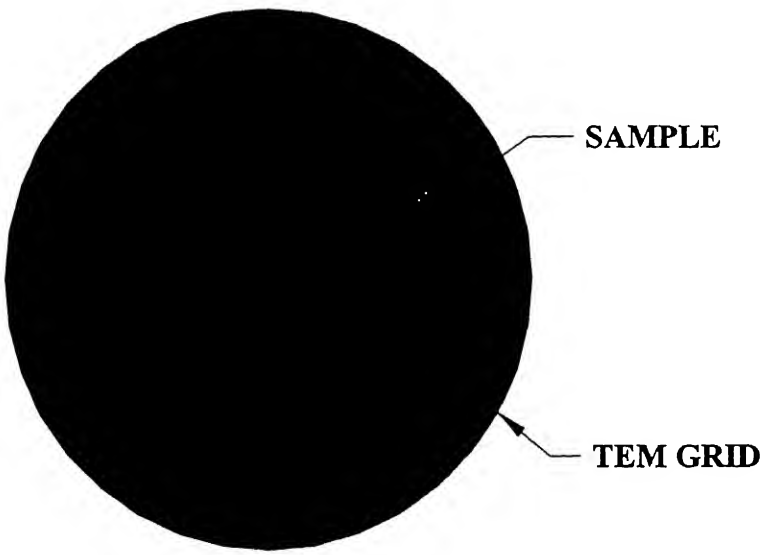


Fig 4.2 (c) Cross sectional TEM disks cut from the Holder.

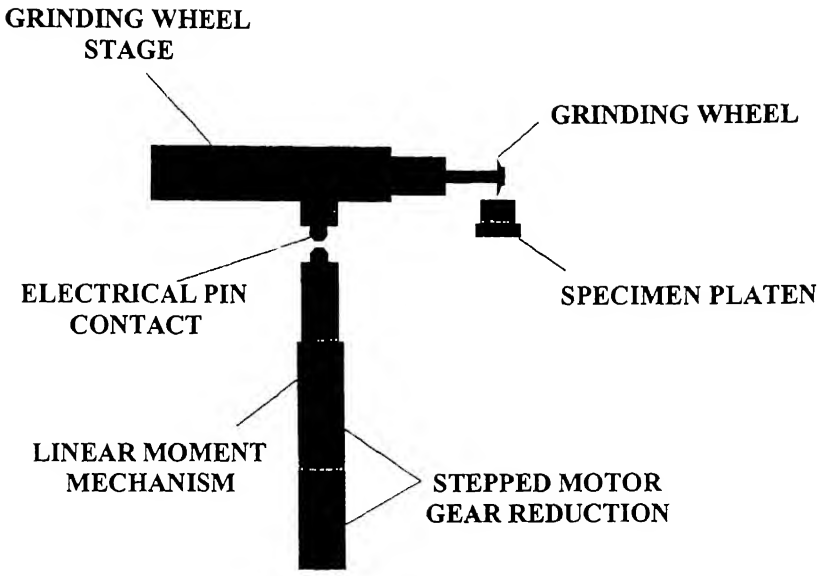


Fig 4.2 (d) Rate control stage of Dimple during dimpling of samples

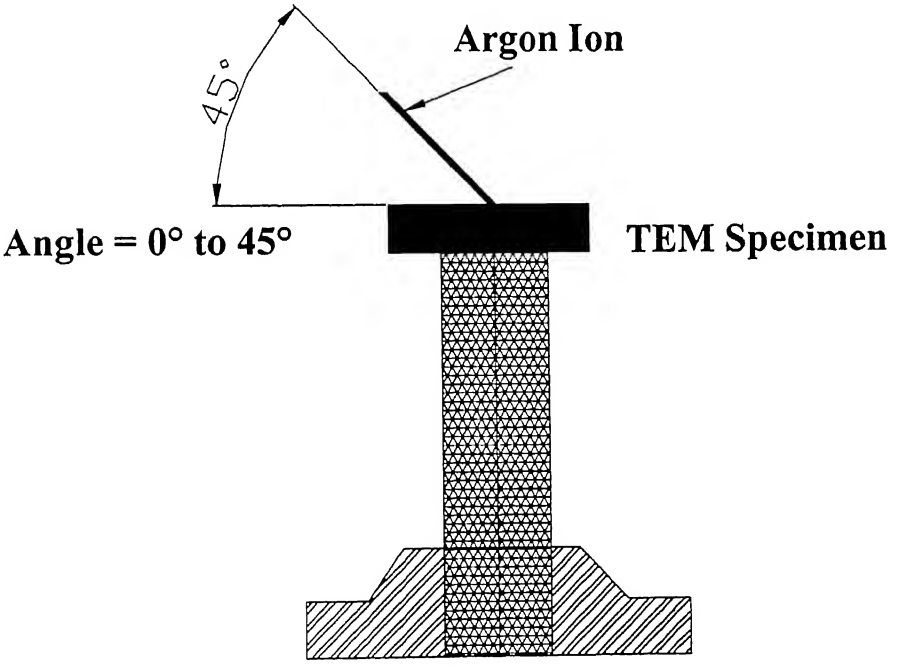


Fig 4.3 Ion milling of $WSi_x$ samples

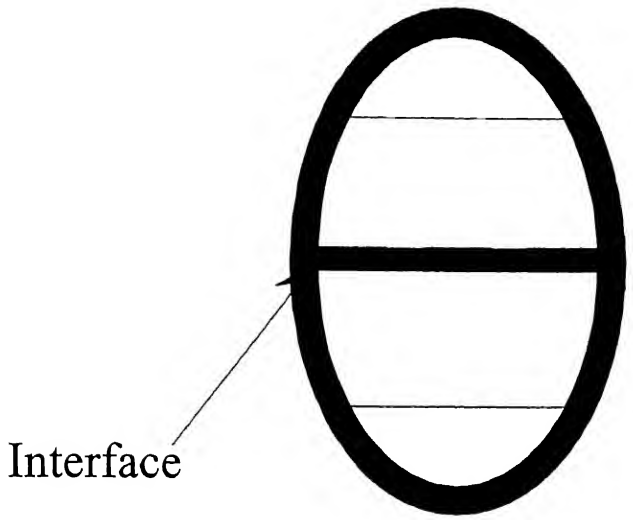


Fig 4.4 Interface of $WSi_x$/Si thin film disk

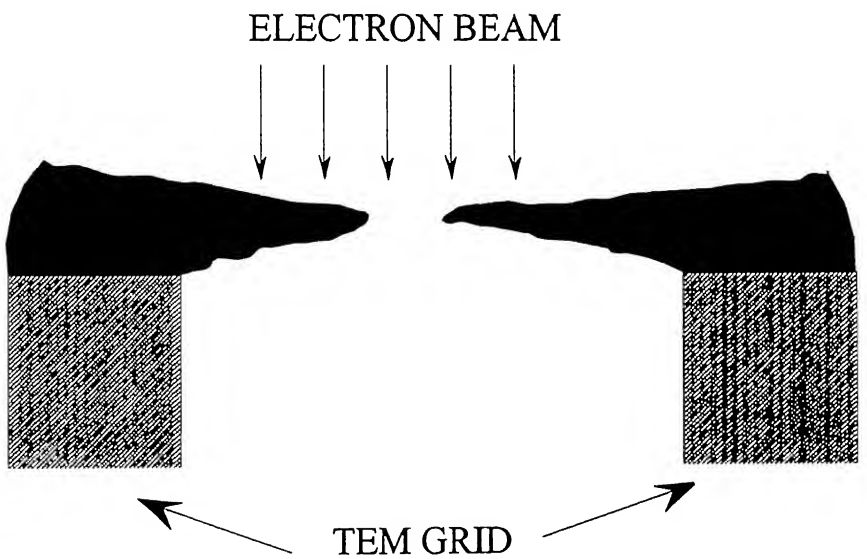


Fig 4.5 Picture of electron transparent area after milling of $WSi_x$ samples.

# CHAPTER 5

# RESULTS AND DISCUSSION

This chapter presents results of various experimental investigations of phase transformation kinetics of $WSi_x$ thin films. The as-deposited and annealed films were studied using resistivity measurement and X-ray diffraction. Rutherford backscattering spectroscopy (RBS) and Cross-sectional TEM studies of the interface are also discussed.

## 5.1 AS-DEPOSITED FILMS

### 5.1.1 THICKNESS MEASUREMENT

In a previous work, thickness and composition of $WSi_x$ films deposited on Si and $SiO_2$ were measured by Rutherford backscattering spectroscopy (RBS) method. Measurements were done under the conditions described in section 3.2.2.[33] The results are summarized here for comparison. Fig 5.1(a) and (b) show the measured values and corresponding simulated values for $WSi_x$/Si and $WSi_x/SiO_2$/Si films, respectively. It was found that tungsten silicide films deposited on both substrates have uniform composition and Si/W ratio (x = 2.4) for both the cases. The thickness of silicides deposited on Si and $SiO_2$ was found to be 5000 ±100 Å and 4650 ±100 Å, respectively.

### 5.1.2 X-RAY ANALYSIS

The X-ray diffraction patterns of $WSi_{2.4}$ films deposited on Si and $SiO_2$ show that as-deposited films are amorphous.

### 5.1.3 RESISTIVITY

The resistivity of $WSi_{2.4}$/Si and $WSi_{2.4}/SiO_2$/Si of thickness 5000 ±100Å and 4650 ±100Å was measured to be 15.2 ± $0.42\times10^{-4}$ Ω-cm and 14.1 ±$0.45\times10^{-4}$ Ω-cm, respectively.

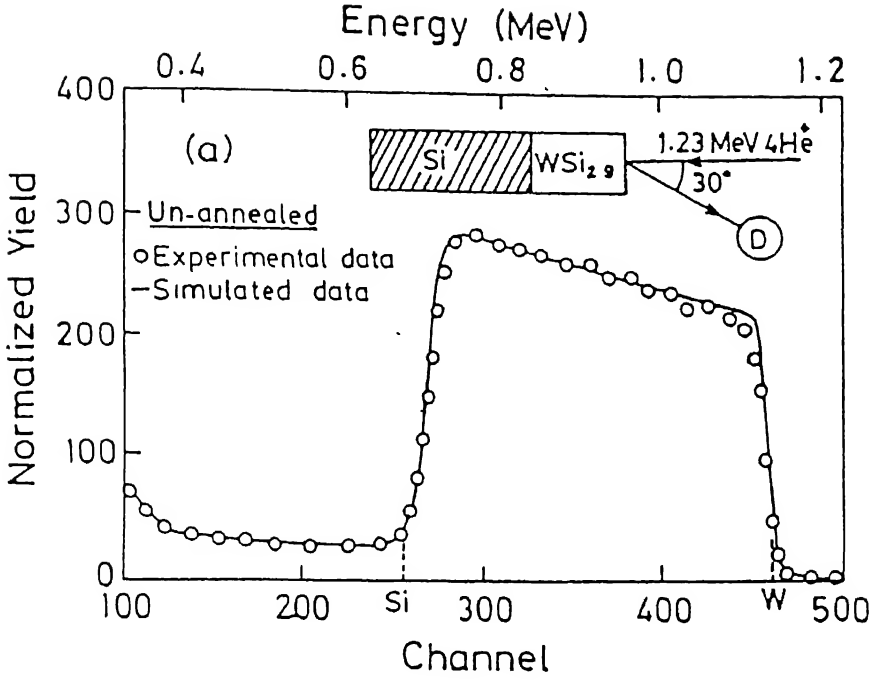


Fig 5.1 (a) RBS analysis of as-deposited $WSi_x$ films on Si.

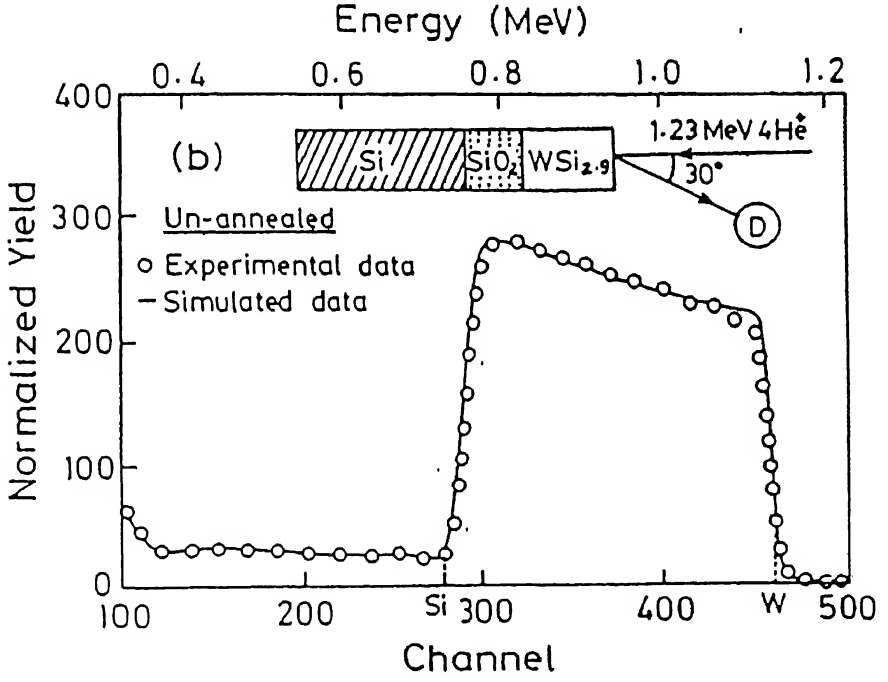


Fig 5.1 (b) RBS analysis of as–deposited $WSi_x$ films on $SiO_2$

## 5.2 RESISTIVITY

Normally, the criterion for deciding annealing process is to achieve lowest sheet resistance/resistivity. As resistivity or sheet resistance is a function of annealing temperature and time, Fig. 5.2 shows how the sheet resistance of $WSi_{2.4}$ varies with annealing temperature for both Si and $SiO_2$ substrate. In this figure it is noticed that due to higher silicon concentration in $WSi_{2.4}$ than $WSi_2$, the resistivity has a maximum value after annealing at 600°C. In this case, the transition from the amorphous state to crystalline state is considered to affect the resistivity behaviour. The high resistance is due to tetragonal $WSi_2$ having very small grain size as discussed in subsequent sections. As the annealing temperature further increases, the film resistivity decreases and attains a minimum saturation value at 1000°C for both Si and $SiO_2$ substrate. It is apparent that the resistivity decreases drastically with in temperature range of 650°C to 1000°C, after which the improvement is very slow or even close to saturation. It is observed that sheet resistance of the film on $SiO_2$ substrate reduces at a faster rate as compared to the sheet resistance of the film on Si substrate. The changes in resistivity as shown in Fig. 5.2 can be understood at the atomic level. The as-deposited film is amorphous and the atoms of tungsten and silicon are randomly distributed throughout the film. Here, it is expected that tungsten atoms are bonded to tungsten atoms, silicon atoms to silicon atoms and also tungsten atom to silicon. When this film is annealed, tungsten atoms bond regularly with silicon atoms. So for that reason the hexagonal structure is crystallized for annealing temperature less than 600°C. The segregation of excess silicon begins around hexagonal $WSi_2$ structure. Consequently, tungsten atoms which are distributed uniformly before annealing, start to be incorporated in the hexagonal $WSi_2$ structure and microstructure of the film changes into $WSi_2$ and excess silicon atoms. Therefore, the conduction mechanism of electrons after annealing differs from the amorphous state, resulting in an increase in resistivity at 600°C. On the other hand, annealing at high temperature results in tetragonal $WSi_2$ structure, the conduction mechanism of electrons is different in this phase resulting in lower resistivity.

Fig 5.3 compares our result having Si/W = 2.4 with the existing literature Si/W = (2.2, 2.6, 3.1) on annealing of $WSi_x$ films on $SiO_2$ substrate. It is interesting to note that the final resistivity, after annealing at 1100°C, of all the films with Si/W

ratio ranging from 2.2 to 3.1 is similar. This means that the electron conduction path is through $WSi_2$ phase, which exist, in the form of large interconnected grains. This is why excess silicon in these films does not affect final resistivity after 1100°C anneal.

Fig. 5.4 shows how the sheet resistance of $WSi_{2.4}$ varies with annealing time at 1000°C for Si and $SiO_2$ substrate. Our results are different from the trends obtained from co-evaporated film, which is shown in the Fig. 5.5. The results in Fig. 5.5 show that there is saturation of sheet resistance after 30 min of annealing for films deposited on polysilicon. But in our case we don't find saturation for 30 min annealing for silicon substrate (annealing behaviour of polysilicon and silicon substarte is assumed to be same). One reason for this could be that our film is rich in Si, where the transformation takes place at higher temperature. It is obvious that 30 min at 1000°C does not represent complete transformation for films on Si substrate; the sheet resistance continues to decrease for annealing times greater than 30 minutes. Some of this difference in the sheet resistance for films on different substrate could be due to the film thickness. We want to emphasize that the decrease of sheet resistance in going from 15 min to 60 min anneal is more for the films on Si as compared to the films on $SiO_2$ substrate. We observe some sort of saturation in the sheet resistance after 30 minutes annealing for films deposited in $SiO_2$ substrate. Here, we are not comparing resistivity of the films as we expect that the thickness is changing with annealing time. Even if we use the initial thickness of the film to convert data into resistivity, the difference in the annealing behavior of the films on different substrates at longer time exists. Next we have to find out weather this difference is in agreement with the X-ray diffraction studies. Once again, it indicates that the phase transformation kinetics of $WSi_x$ is dependent on the type of the substrate.

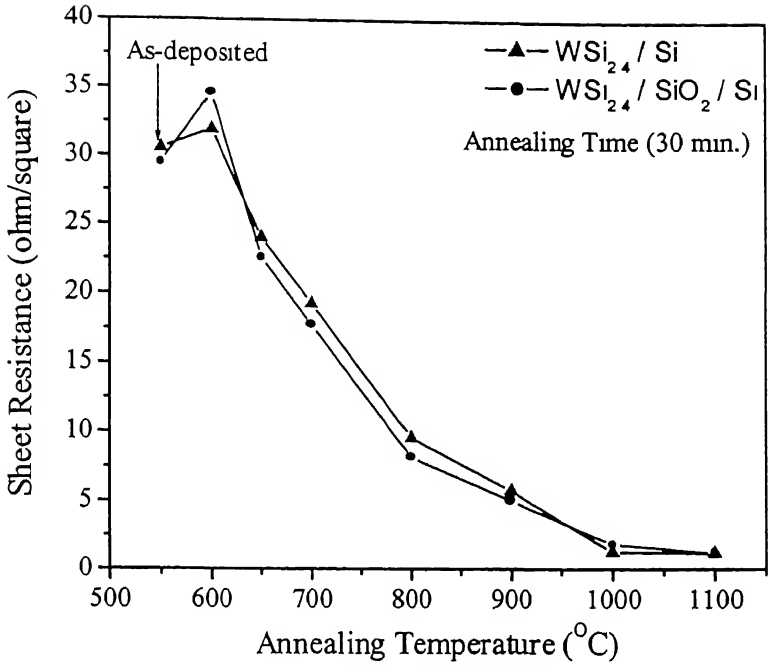


Fig.5.2 Change in the sheet resistance of $WSi_{2.4}$ films as a function of annealing temperature.

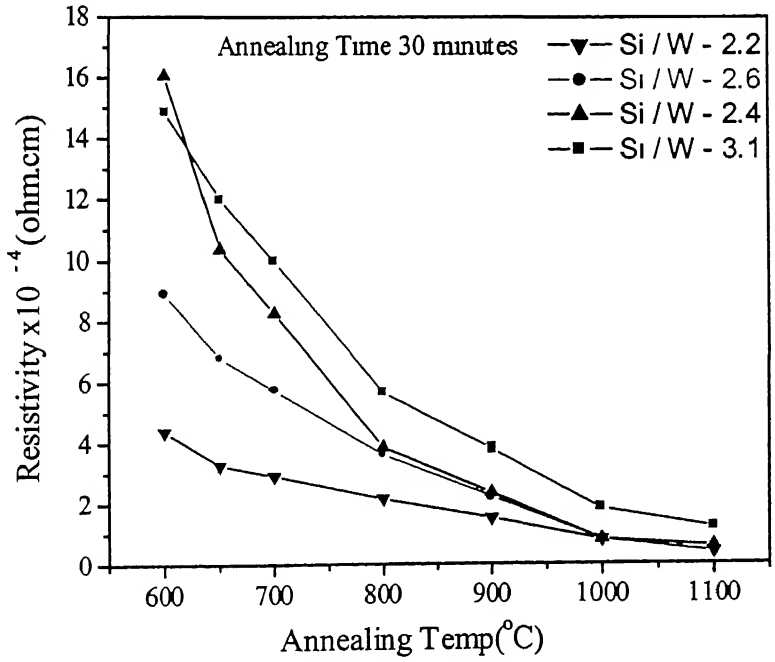


Fig 5.3 Change in the resistivity of $WSi_x$ (Si/W = 2.2, 2.6, 2.4, 3.1) films deposited on$SiO_2$ substrate as a function of annealing temperature and anneal time 30 min.

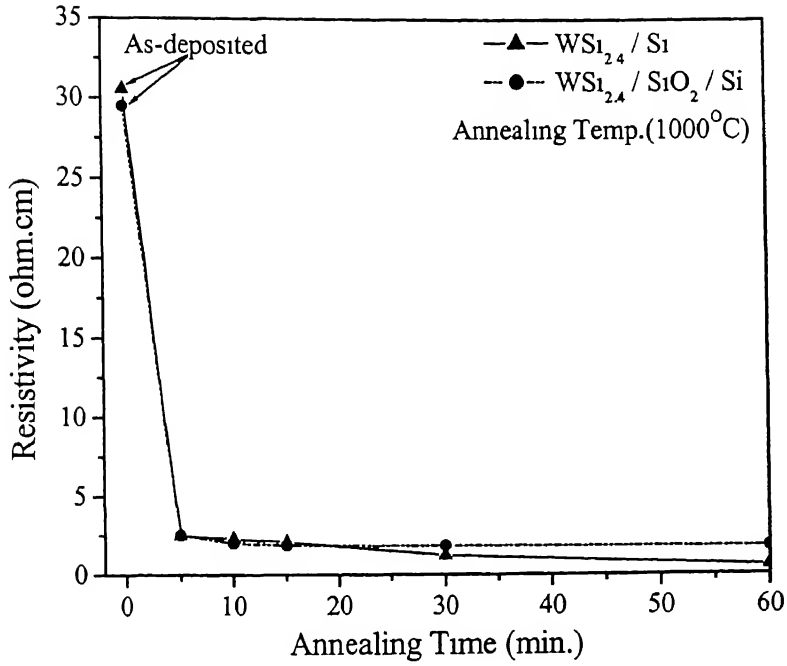


Fig 5.4 Sheet resistance of $WSi_{2.4}$ films deposited on Si and $SiO_2$ substrates, as a function of annealing time, annealing is done at 1000°C.

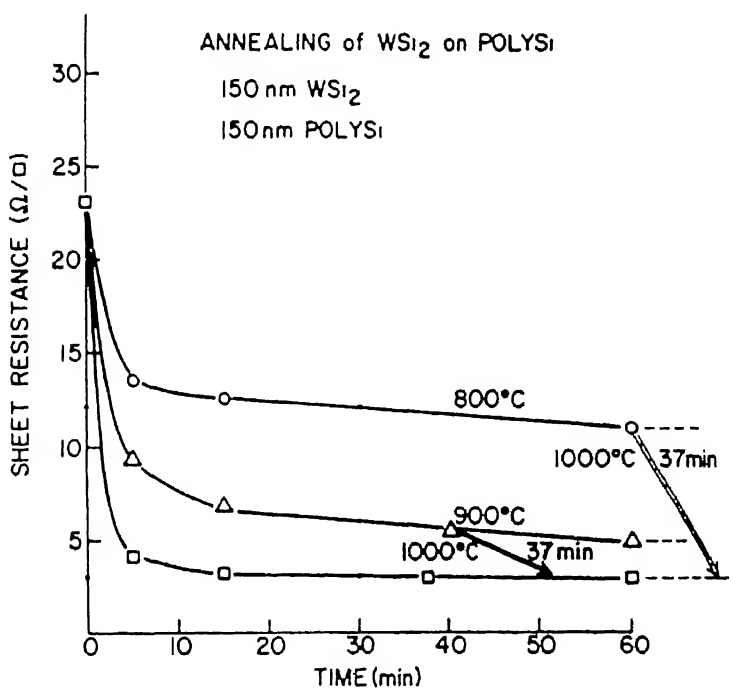


Fig 5.5 Change in sheet resistance of co-evaporated $WSi_2$ films deposited on poly-Si as a function of annealing temperature and time.

## 5.3 X-RAY DIFFRACTION

The X-ray diffraction patterns of $WSi_{2.4}$ films, deposited on Si and $SiO_2$, annealed at different temperatures for 30 minutes are presented in Fig 5.6 (a) and (b). After 30-minutes anneal at 450°C and 500°C, both types of samples are peeled off and cracked. This effect is more in $WSi_{2.4}$/SiO2/Si as compared to $WSi_{2.4}$/Si. This problem is due to high internal strains developed in the films due to crystallization at that temperature. The diffraction patterns obtained at 550°C temperature show a weak hexagonal peak at 2θ value of 41.46°. As annealing temperature further increases; at around 600°C there is no evidence of hexagonal peak. The diffraction patterns corresponding to anneal at 600°C in both the case show that a well-defined structure of $WSi_2$ tetragonal structure is starting to crystallize. For this reason, high resistance of this film is attributed to fine grains of the tetragonal phase.

The tetragonal phase is crystallized along the planes (002),(101),(110),(103) and (112) having 2θ value at 22.72°, 30.06°, 39.67°, 44.83°, 46.22°. In both the cases, as annealing temperature further increases, at 800°C an additional tetragonal peak for (200) plane at 57.3° appears. Diffraction peaks are quite sharp and the widths decrease with increasing annealing temperature, this indicates that degree of crystallization is more and grain size is also large for high temperature anneals. Since, relative intensities of the diffraction peaks match the expected value for the powder diffraction pattern of the tetragonal structure given in table 5.1, there is no preferred texture in the crystallized films. Fig 5.7 (a) and (b) show how the X-ray diffraction intensity of different peaks varies with time during 1000°C anneal of $WSi_{2.4}$/Si and $WSi_{2.4}$/$SiO_2$/Si films. During annealing amorphous $WSi_{2.4}$ is being transformed to $WSi_2$, we do not detect other phases of tungsten silicide at this temperature

TABLE 5.1

Calculated relative intensity for powder diffraction pattern of $WSi_2$ tetragonal phase

| 2θ value (degree) | Diffracted plane (hkl) | Relative intensity (arb.units) |
|---|---|---|
| 30.063 | (101) | 100 |
| 44.832 | (103) | 85 |
| 39.672 | (110) | 70 |
| 46.223 | (112) | 50 |
| 22.723 | (002) | 50 |
| 57.4 | (200) | 25 |

Time–resolved X-ray diffraction can be used to study the kinetics of phase transformation, if the peak intensity is proportional to the amount of phase formed. This condition is satisfied in our case as films are only 0.5 and .465 micron thick and $CuK_\alpha$ beam samples the full thickness of the film with less than 10% absorption in the film. Fig 5.8 (a) and (b) plots the integrated intensity of diffraction peaks for Si and $SiO_2$ substrates as a function of annealing temperature. This integrated intensity is calculated taking the area under each peak. As expected for $WSi_{2.4}/SiO_2/Si$, the peak intensity continuously increases as degree of crystallization increases, while for $WSi_{2.4}/Si$ the intensity increase is not linear. This is in agreement with the observation of faster decrease in resistivity in $WSi_{2.4}/SiO_2/Si$. It also indicates complication in directly relating the crystallized phase with the measured resistivity.

Fig. 5.9 (a) and (b) plots the integrated intensity of diffraction peaks as a function of annealing time at 1000°C for both substrates. Once again, the behavior upto 15 minutes indicates faster phase transformation on $SiO_2$ substrate. Beyond 15 minutes, the peak intensities show a small change for the oxidized substrate and a bigger change for the Si substrate. This is in agreement with the sheet resistance data in Fig. 5.4. Sheet resistance for films on $SiO_2$ substrate is nearing saturation at 15 minutes annealing because phase transformation is complete, and there are no changes in the structure beyond that. On the other hand, sheet resistance on Si substrate continues to reduce as phase transformation is still going on beyond 15 minutes. The total kinetic of phase transformation will be discussed in the chapter 6. Fig. 5.10 plots

the sum of all diffraction peaks intensity as a function of annealing time at 1000°C. Although this was not very clear from the resistivity plot X-ray information shows clear difference in the phase transformation kinetics on Si and $SiO_2$ substrate. This difference is probably due to the diffusion of excess silicon to the $WSi_{2.4}$/Si interface. More details on this can be obtained only by TEM studies as a function of annealing time and temperature.

## 5.4 PROCEDURE OF GRAIN SIZE MEASUREMENT

Average grain size of annealed $WSi_x$/Si and $WSi_x/SiO_2$/Si thin films was calculated by Debye Scherer formulae by using the measurement of full width at half maximum (FWHM). Grain size was calculated by measuring the broadening of a particular peak in a diffraction pattern associated with a particular planar reflection of the crystal. It is inversely related to the FWHM of an individual peak, the more narrow the peak, the larger the grain size. In our experiment, we found out that for both $WSi_x$/Si and $WSi_x/SiO_2$/Si films the FWHM decreases with increasing annealing temperature, which is shown in the Fig 5.6 (a) and (b). At 1000°C, the peaks are narrower as annealing time increases

To measure the grain size, a diffraction pattern from the specimen was collected. A background was subtracted and the peak profile was fitted to measure the area under the curve and FWHM. If breadth of diffraction line at half of its maximum intensity (or peak height) measured in radians is 'B' at a particular Bragg angle θ (corresponding at 2θ in the diffractogram), the grain size <D> of the annealed $WSi_x$ film is given by the Scherer formulae.

$$\langle D \rangle = \frac{0.9\lambda}{B\cos\theta}. \qquad 5.1$$

Where, ⟨D⟩ = Average grain size

λ = X-ray wave length ($1.5418A^0$)

B = the width of half amplitude

θ = Bragg's angle

The breadth 'B' in the above formulae refers to broadening due to grain size alone. In addition, the diffractometer can also introduce a small amount of peak broadening. This inherent broadening is known as the instrumental broadening. This happens only due to incident beam divergence and sample size (for Debye Scherer cameras) and

width of the X- ray source (for diffractometer). This type of broadening is present in the sample having grain size exceeding 0.1-0.2 μm. It is necessary to make appropriate corrections in the experimentally measured breadth $B_m$'s of diffraction lines. So, for that reason we have taken diffraction pattern of standardized crystalline sample Si that was recorded under specified experimental conditions. The peak contains sharp lines. The breadth 'b' was measured at half maximum and plotted against the respective angle 2θ to get a correction curve. The diffraction pattern of the annealed $WSi_x/Si$ and $WSi_x/SiO_2/Si$ was recorded under identical conditions and breadth '$B_m$' was measured at half of the maximum intensity. Using the $B_m$ vs.2θ plot of the standard sample, appropriate value of instrumental broadening was found for each 2θ angle of diffraction line. A reference FWHM parabolic curve that was generated from the standard silicon crystalline sample was subtracted from the specimen pattern. As the intensity profile follows a Gaussian distribution, so the breadth 'B' was calculated as follows:

$$B = \sqrt{B_m^{\,2}} - b^2$$

All the grain size calculations were determined using the Scherer formula once the corrected FWHM was known. The Scherer equation yields the grain size for a specific peak, we have calculated the average grain size which was determined by multiple peaks.

The relationship between the grain size and the resistivity is important to study the phase transformation kinetics of $WSi_{2.4}$ films deposited on Si and $SiO_2$ substrate. Fig 5.11 shows the relationship between the resistivity and inverse of grain size at different temperatures. Resistivity decreases monotonically with respect to inverse of grain size. It shows that grain size increases as temperature increases, where as the resistivity decreases. Therefore, the decrease of resistivity is due to increase of grain size at higher anneal temperatures. The same trend is seen for $WSi_{2.4}/SiO_2/Si$ substrate as shown in Fig.5.12. Fig. 5.13 shows the average grain size as a function of annealing temperature. Grain size increases upto annealing temperature of 1000°C. There is no change in the grain size beyond that temperature. So that means there is complete phase transformation at 1000°C, this is consistent with the resisitivity data. It is noted that grain size on the $WSi_x/SiO_2/Si$ is more than $WSi_x/Si$ below 900°C, but

at higher temperatures the grain size on Si substarte is more. The reason behind this phenomenon is that $SiO_2$, acts as barrier for diffusion of silicon, and the grain growth phenomenon ceases for these films. On the other hand, on Si substrate excess Si can diffuse to the interface and assist further growth of the grains at higher temperatures.

Fig 5.14 shows the relationship between the average grain size and annealing time for $WSi_{2.4}/Si$ and $WSi_{2.4}/SiO_2/Si$ at 1000°C. It reveals that for $WSi_{2.4}/Si$ substrate, as annealing time increases the grain size increases. This happens up to 60 min of annealing. So, the results show incomplete phase transformation even if at higher time. Here, grain growth occurs for longer annealing times at 1000°C. This indicates more diffusion of silicon to the interface and reduced segregation of Si at the grain boundaries. But for $WSi_{2.4}/SiO_2/Si$ substrate grain growth is over at 15 min of annealing. After 30 minutes annealing the grain size remains constant similar to resistivity and X-ray intensity results. This infers that there is no diffusion of Si to the interface for $SiO_2$ substrate, and no change in the film microstructure after 15 minutes anneal at 1000°C. More details we can be found out from the cross sectional TEM study of annealed samples.

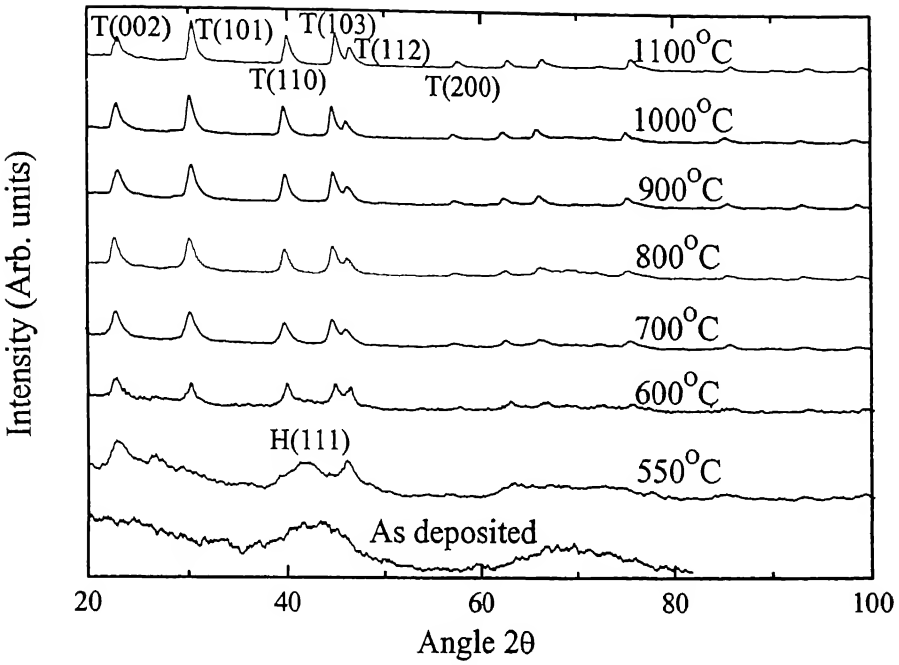


Fig 5.6 (a) Change in X-ray intensity of $WSi_{2.4}$ films deposited on Si as a function of annealing temperature for constant time 30 min

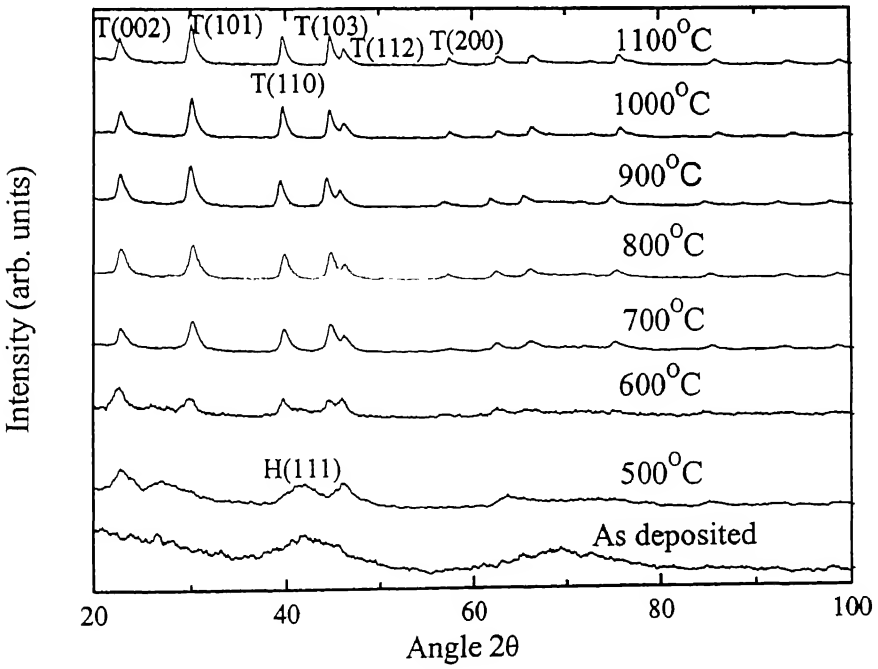


Fig.5.6 (b) Change in the X-ray intensity of $WSi_{2.4}$ films deposited on $SiO_2$ substrateas a function of annealing temperature for constant time 30 min

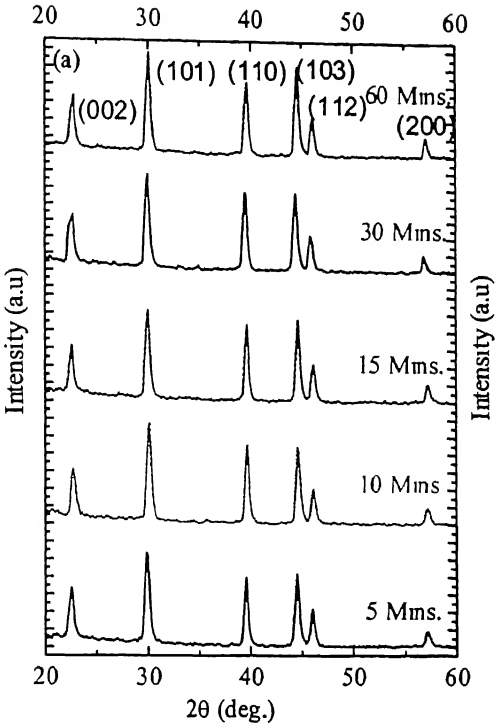


Fig.5.7 (a) Change in X-ray intensity of $WSi_{2.4}$ film deposited on Si as a function of annealing time at constant temperature 1000°C

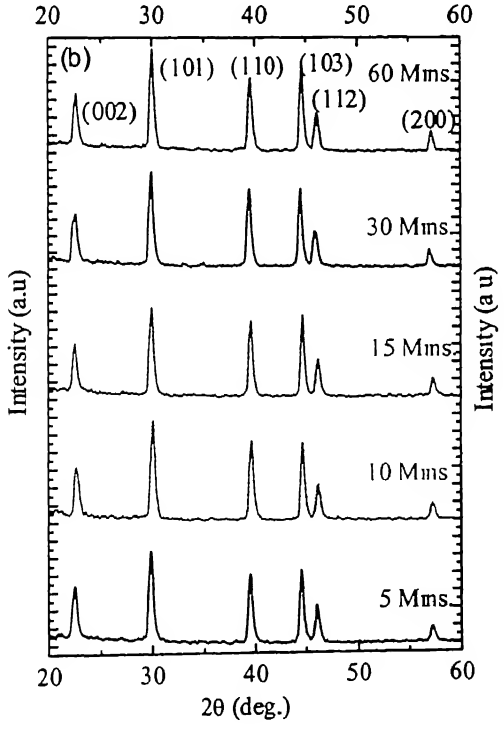


Fig.5.7 (b) Change in X-ray intensity of $WSi_{2.4}$ film deposited on $SiO_2$ as a function of annealing time at constant temperature 1000°C

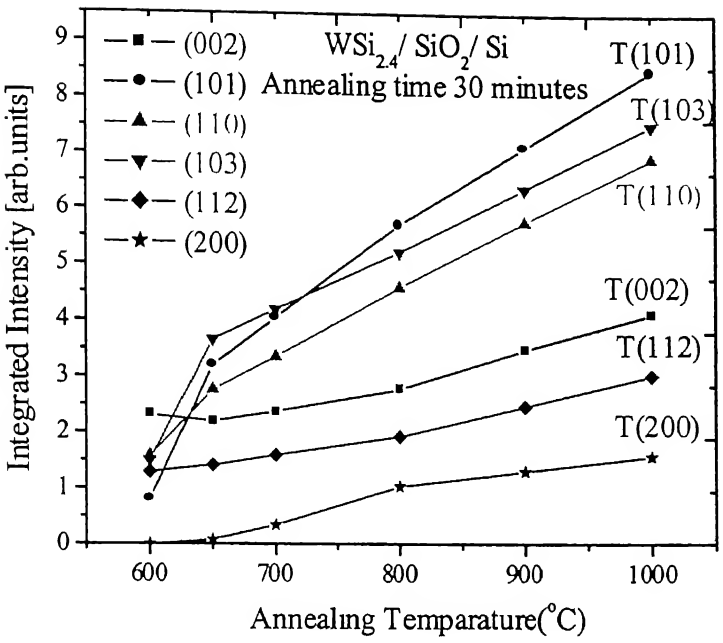


Fig.5.8 (a) Integrated X-ray intensity of diffraction peaks of $WSi_{2.4}$ films, deposited on Si substrate as a function of annealing temperature at constant time 30 min

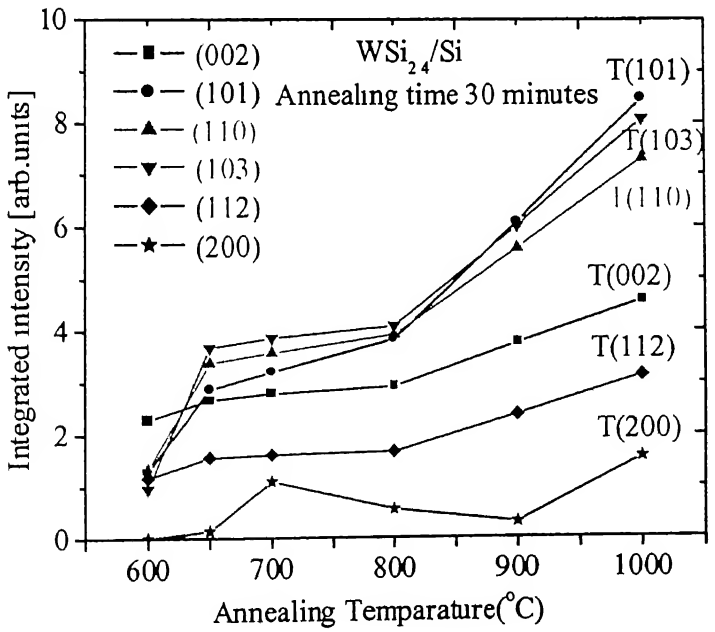


Fig 5.8 (b) Integrated X-ray intensity of diffraction peaks of $WSi_{2.4}$ films, deposited on. $SiO_2$ substrate as a function of annealing temperature at constant time 30 min

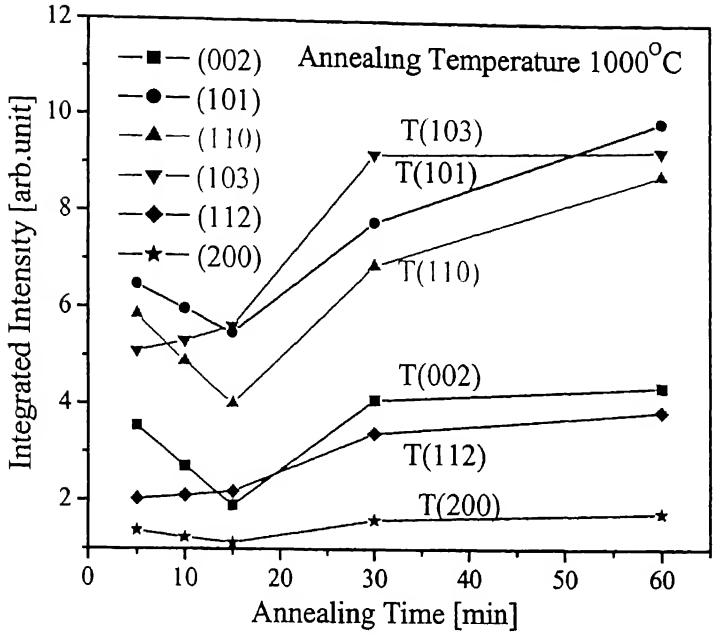


Fig.5.9 (a) Integrated X-ray intensity of diffraction peaks of $WSi_{2.4}$ films, deposited on Si substrate as a function of annealing time at constant temperature 1000°C

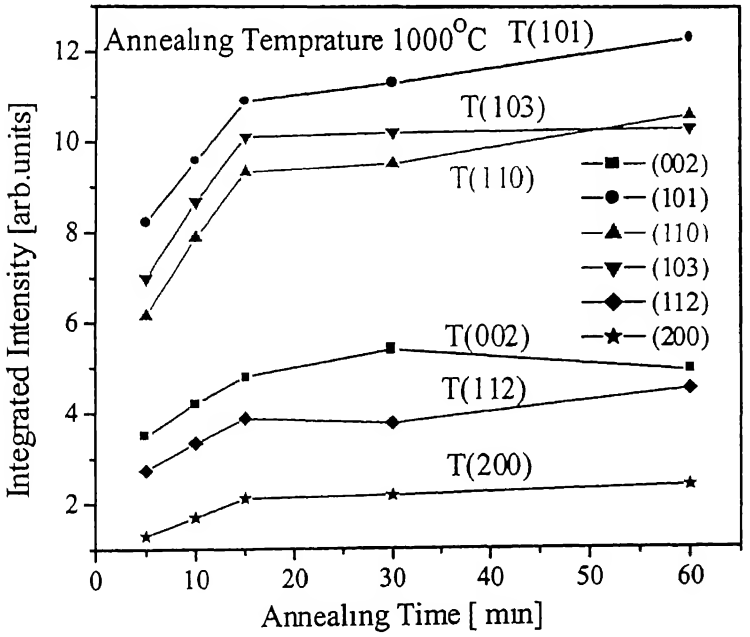


Fig.5.9 (b) Integrated X-ray intensity of diffraction peaks of $WSi_{2.4}$ films, deposited on $SiO_2$ substrate as a function of annealing time at constant temperature 1000°C

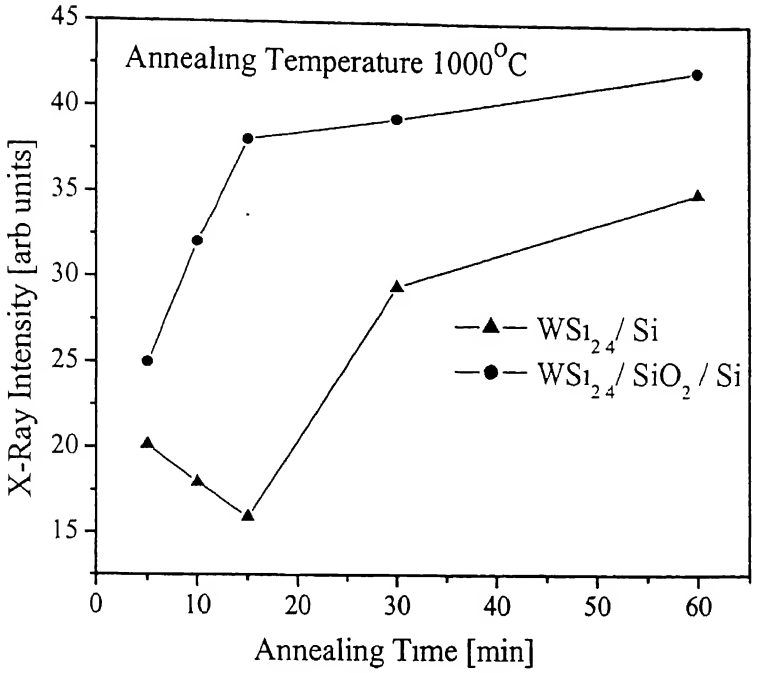


Fig.5.10.Change in the sum of integrated X-ray Intensity of diffracted plane as a function of annealing time at constant temperature of 1000°C

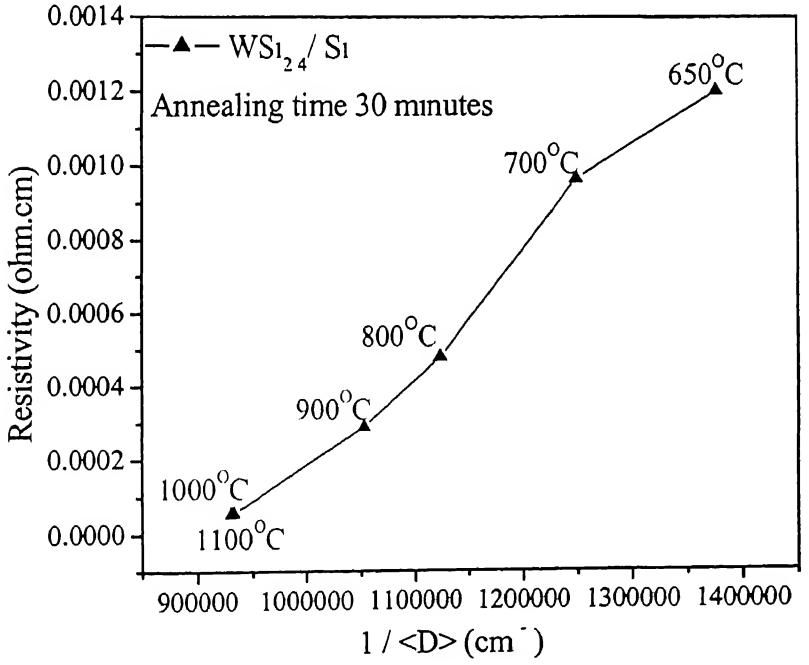


Fig 5.11 Relation between resistivity and average grain size of tetragonal $WSi_2$/Si film at various temperatures

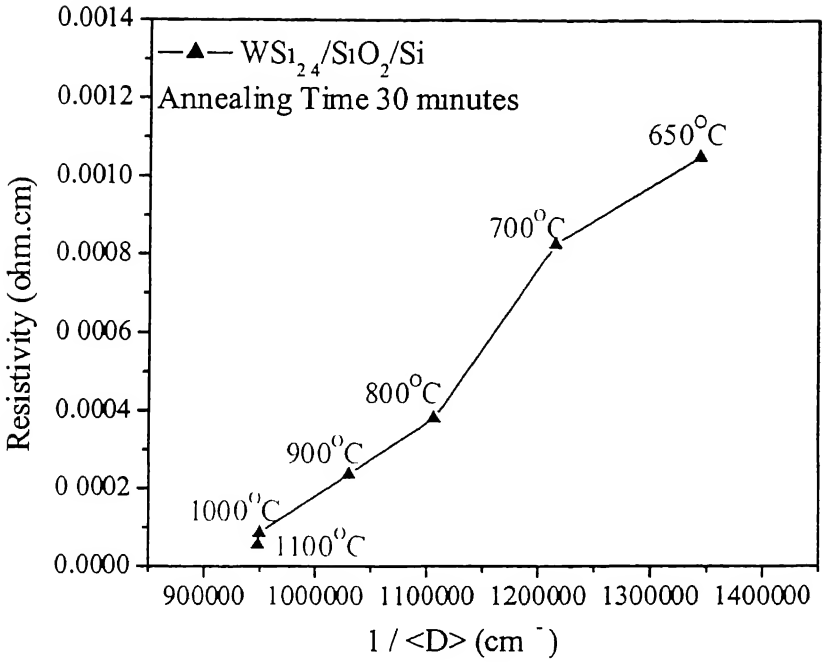


Fig 5.12 Relation between resistivity and inverse of average grain size of tetragonal $WSi_{2.4}/SiO_2/Si$ film

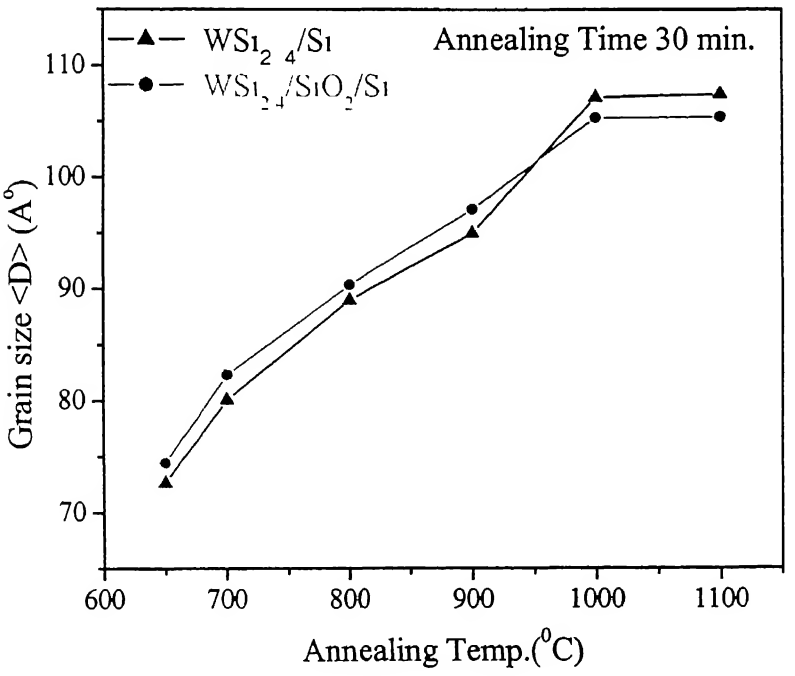


Fig 5.13 Relation between average grain size of tetragonal$WSi_{2.4}/Si$ and $WSi_{2.4}/SiO_2/Si$ film and annealing temperature at constant time30 min

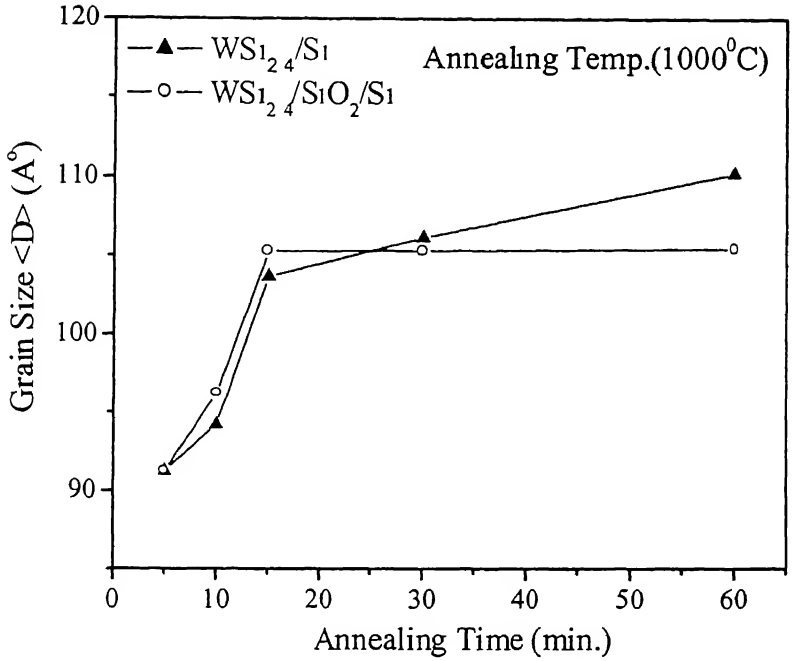


Fig 5.14 Relation between average grain size of tetragonal $WSi_{2.4}$/Si and $WSi_{2.4}/SiO_2$/Si film and annealing time at 1000°C

## 5.5 CROSS-SECTION TEM IMAGES

The (100) oriented cross sectional TEM specimens were prepared by dimpling followed by Ion milling. The crystal structure and the crystallization of the films were characterized at 100, 50 kV on a JEM 200 FX (JEOL) electron microscope, which is set up in ACMS IIT Kanpur. In Fig 5.15(a), for a sample annealed at 700°C for 0.5hr, it is revealed that a number of grains with average diameter of about 80nm formed at the silicide phase at 100kV. In the same figure corresponding electron diffraction patterns also shows that the crystal structure is almost. in tetragonal form. This figure also gives some idea about the diffusion of silicon towards the interface from substrate, which is indicated by arrow marks. Fig 5.15(b) shows a number of grains with average diameter 40nm formed at the silicide phase at 50kV. This picture has taken from the same sample, which were annealed at 700°C for 0.5hr.The arrowhead indicates that excessive silicon atoms are segregated at the silicide/silicon interface during the annealing.

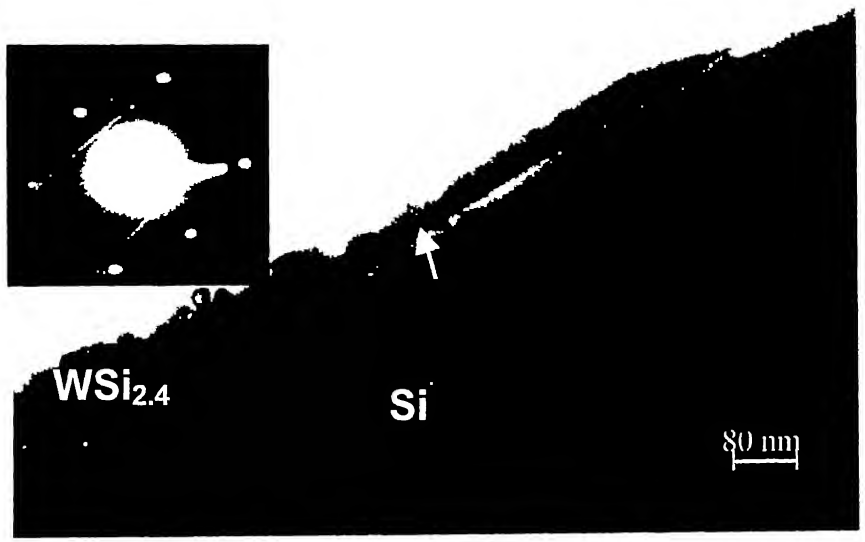


Fig 5.15 (a) Cross-sectional view of $WSi_{2.4}$/Si after annealing at 700°C for 30 min $N_2$, in which grain growth occurs due to the segregation of Silicon is indicated by an arrow. The electron diffraction patterns are also shown in the outsets

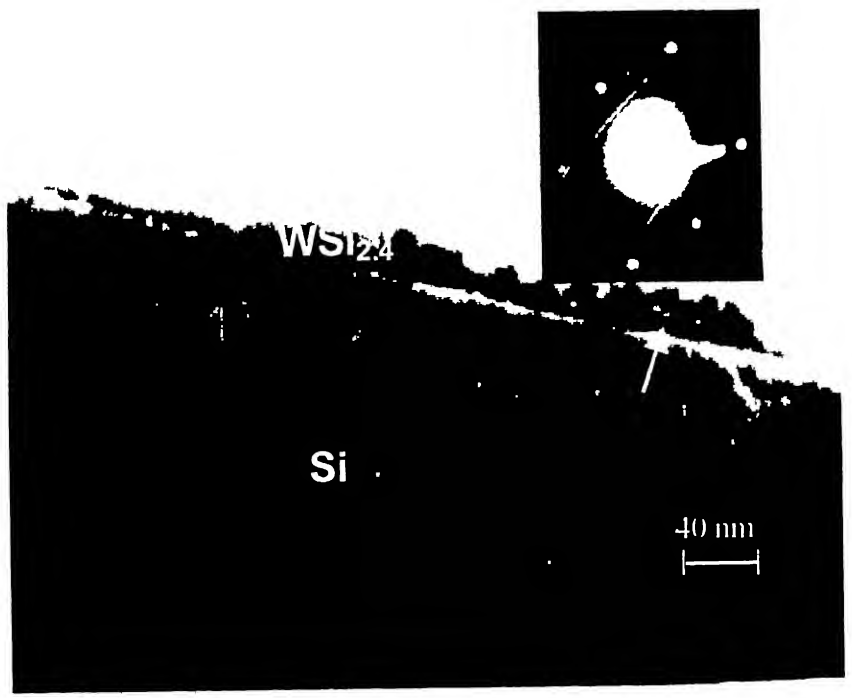


Fig 5.15 (b) Cross-sectional view of $WSi_{2.4}$/Si after annealing at 700°C for 30 min $N_2$, in which grain growth occurs due to the segregation of Silicon is indicated by an arrow. The electron diffraction patterns are also shown in the outsets

# CHAPTER 6

## KINETICS OF PHASE TRANSFORMATION

In this chapter, I present the thermodynamic and kinetic aspects of amorphous to tetragonal transformation in $WSi_x$ thin films.

### 6.1 THERMODYNAMICS OF $WSi_2$ FORMATION

First we need to consider the thermodynamic feasibility of the following reaction:

Amorphous ($WSi_x$)→Tetragonal ($WSi_2$)

Reports of thermodynamic investigations of $WSi_2$ have appeared in the literature.[32] At high temperatures Borisenko reported the enthalpy value in the form of a polynomial for the temperature range 1200 - 2200 K.

$$\Delta H^{T}_{298}\ (\text{J/mol}) = 34.294T + 15.421\times 10^{-3}T^{2} - 5.864\times 10^{6}\,T^{-1} + 8074 \qquad 6.1$$

The corresponding molar heat capacities is given by the differentiation as

$$C^{o}_{p,\,m} / (\text{J.K}^{-1}\,\text{mol}^{-1}) = 34.294 + 30.842\times 10^{-3}T + 5.864\times 10^{6}\,T^{-2} \qquad 6.2$$

To date molar entropy increase $\Delta S^{T}_{298}$ has not been determined experimentally; Borisenko derived the following expression by conventional thermodynamic manipulations:

$$\Delta S^{T}_{298} / \text{J.K}^{-1}\,\text{mole}^{-1} = 34.294\ln T + 30.842\times 10^{-3}\,T - 2.932\times 10^{6}\,T^{-2} - 252.3125 \qquad 6.3$$

So, from the above equations we derived the free energy $\Delta G^{T}_{298}$ of $WSi_2$

$$\Delta G^{T}_{298} = \Delta H^{T}_{298} - T\Delta S^{T}_{298} \qquad 6.4$$

$$\Delta G^{T}_{298} = 34.294\times T\,(1 - \ln T) - 15.421\times 10^{-3}T^{2} - 2.932\times 10^{6}\,T^{-1} + 8074 + 252.3125\times T \qquad 6.5$$

Table 4 shows the values of $\Delta H^T$, $\Delta S^T$, $\Delta G^T$ Of $WSi_2$ at different temperatures.

**TABLE 6.1.**

Calculated values of $\Delta G^T$ at different temperatures.

| Temperature ($^oK$) | ($-\Delta H^T$ (J/mole)) | ($-\Delta S^T$ (J/mole/K)) | $-\Delta G^T$ (J/mole) |
|---|---|---|---|
| 1223 | -67859.4644 | -26.8612 | 35008.2168 |
| 1273 | -72113.9976 | -30.3124 | 33526.3124 |
| 1323 | -76004.4347 | -33.3448 | 31889.15 |
| 1373 | -79959.2964 | -36.2152 | 30235.8268 |

As $\Delta G^T < 0$ , the formation of unlike bonds is preferred - W and Si atoms show a preference to become nearest neighbours The table shows that change in enthalpy $\Delta G^T$ decreases as the temperature increases. Therefore, driving force for phase transformation is more at higher temperatures.

## 6.2 KINETICS OF PHASE TRANSFORMATION OF $WSi_x$

Based on the thermodynamic consideration, we expect that crystallization of $WSi_2$ from amorphous $WSi_x$ will occur by nucleation and growth process. The transformation can be divided into two steps that occur sequentially.

i) The formations of tiny particles that are stable to further thermal fluctuations and will not dissolve.

ii) The increase in size of these particles.

Step (1) is called nucleation and step (2) is growth. The interface that separates two phases has a surface energy; this energy has to be supplied during nucleation. The rate of nucleation and growth determines the grain size of the product phase. The combination of high nucleation and a low growth rate yields a fine grain size. On the other hand, a low nucleation rate combined with high growth rate yields a coarse grain.

When the mechanism of transformation is that of nucleation and growth, the kinetics of transformation can be described by the Avarami relationship.

$X_T(t). = 1\text{-}exp\ [(-Kt)^n]$ 6.7

Where, $t$ The actual transformation time after the incubation period.

K → Rate constant, which is function of growth parameter, density of nucleation sites

'$n$' The time exponent (growth parameter) depends on the nature of nucleation and growth process, which can be determined from the plot of

$ln\ ln\ [1\text{-}X_T(t)]^{-1}$ vs. $ln\ t$.

Table6.2 gives the expected values of 'n' under different conditions of transformation. From the table it is confirmed that the time exponent value 'n' differs for different transformation conditions,and can be used to infer the nucleation and growth mechanism.

**TABLE 6.2**

Value of time exponent 'n' for different transformation conditions

| Transformation conditions | Value of n | |
|---|---|---|
| | Constant growth | Parabolic growth |
| Increasing nucleation rate (random nucleation) | >4 | >2.5 |
| Constant nucleation rate (random nucleation) | 4 | 2.5 |
| Decreasing nucleation rate (random nucleation) | 3-4 | 1.5-2.5 |
| Zero nucleation rate (early site saturation, random nucleation) | 3 | 1.5 |
| Grain edge nucleation (early site saturation) | 2 | 1 |
| Grain boundary nucleation (early site saturation) | 1 | 0.5 |

Nava et al first studied the kinetics of phase transformation in 1987.[] According to them, the phase transformation for both amorphous to hexagonal and hexagonal to tetragonal, the mode parameter 'n' is approximately 2. They had studied phase transformation in co-evaporated $WSi_x$.

In our case, the CVD deposited $WSi_x$ film on Si and $SiO_2$ substrates have different resistivity in transformed and untransformed structures. The change in sheet resistance or resitivity was achieved at isothermal temperature of 1000°C for different times like 5, 10, 15, 30, 60 minutes. The time dependence of the transformed volume

fraction, assuming a linear relationship between the instantaneous sheet resistance $\rho(t)$ and volume fraction of the isothermally transformed material $X_T(t)$

$$X_T(t) = \frac{(\rho_\alpha - \rho_t)}{(\rho_{\alpha-}\rho_\beta)} \qquad 6.6$$

Where $\rho_\alpha$ and $\rho_\beta$ are sheet resistance of the initial and final phases respectively. In this experiment, we have found the value of 'n' for phase transformation at 1000°C. Table 6.3 shows the values of 'n' for $WSi_x/Si$ and $WSi_x/SiO_2/Si$ films at 1000°C.

**TABLE 6.3**

Value of time exponent 'n' of annealed $WSi_x/Si$ and $WSi_x/SiO_2/Si$ at 1000°C for different time conditions

| Time range | $n_{Si}$ | $n_{SiO2}$ |
|---|---|---|
| 0-5 | 1.36 | 1.23 |
| 5-60 | 0.34 | 0.33 |

### 6.2.1 $WSi_x/Si$ films

In Fig. 6.1, it is observed that phase transformation kinetics for $WSi_x/Si$ films in first 5 min is different compared from last 55 minutes. The growth parameter value 'n' at the beginning i.e. in between 0-5 minutes is found to be 1.36. Looking at table 6.2, this indicates random nucleation and parabolic growth.

Thermally activated growth occurs by random motion of individual atoms across the parent/product interfaces. When there is no change in composition during the transformation, growth is controlled by short-range movement of atoms across the interface and is called as interface controlled growth. However, when the composition of the product phase is different from that of parent phase, long range diffusion of solute to or away from the interface is also required in addition to transfer of atoms across the interface. The growth may be then controlled by

i. The rate at which solute atoms diffuse to (or away from) the interface (diffusion controlled growth).

ii. The rate at which the atoms moves across the interface (interface controlled growth)

iii. Mixed of these two phenomenon

As the composition of $WSi_{2.4}$/Si (parent phase) is different from $WSi_2$/Si (product phase) during $WSi_{2.4}$ $WSi_2$ transformation in a binary W-Si system, diffusion of solute Si in $WSi_{2.4}$ or away from the interface is required for the growth of $WSi_2$ phase.[30,31,32] Under these conditions, growth of $WSi_2$ phase may be controlled by rate of solute diffusion away from the interface. Therefore, parabolic growth mechanism is consistent with our observation of n being equal to 1.36, which is close to 1.5. The value of n also depends on the geometry and spatial distribution, as these determine the boundary conditions for solute diffusion.

The growth parameter 'n' decreases for annealing beyond 5 miutes, it is 0.34 as shown in Fig 6.1. It indicates that, the nucleation is showing early site saturation after first five min, and only growth of the existing grains is taking place in this zone. As far as $WSi_x$/Si films are concerned, it is observed, from the RBS results, that the composition of $WSi_{2.4}$ changes to $WSi_2$ after annealing at $1000^0$C for 60 minutes. The excess Si must be going to the interface as seen in the TEM images. Therefore, growth phenomenon is predicted to be long-range diffusion controlled. Further growth of the grains has to be accompanied with the Si diffusion to the interface.

### 6.2.2 $WSi_x/SiO_2$/Si films

The growth parameter value 'n' for $WSi_x/SiO_2$/Si at the beginning i.e for first 5 minutes is found to be 1.23, which is shown in Fig. 6.2. This is similar to the value obtained for $WSi_x$/Si films. This indicates random nucleation and parabolic growth.

The growth parameter decreases with time and found to be 0.33 beyond 5 min as shown in Fig 6.2. It indicates the zero nucleation rate (early site satuaration) and grain growth controlled by long range diffusion of excess Si.

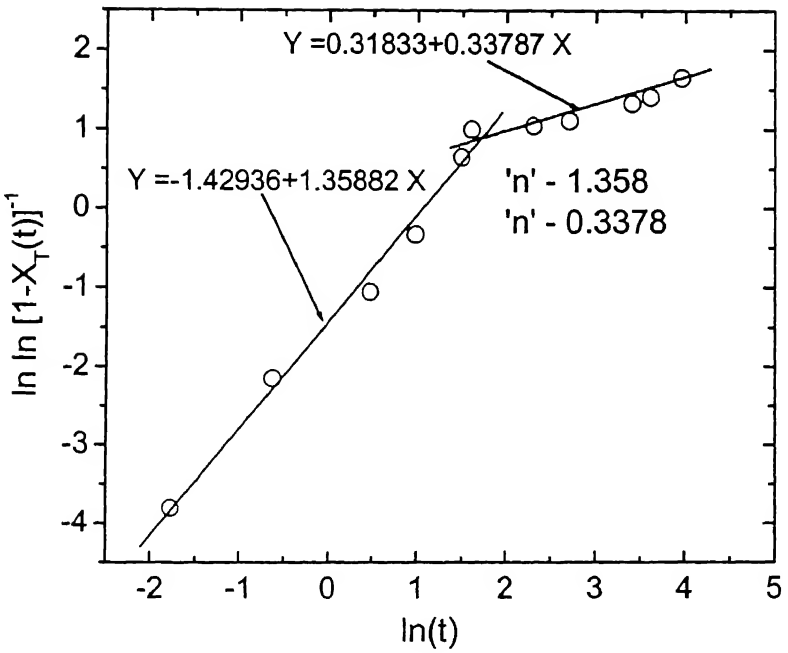


Fig 6.1 Fitting curve shows the growth parameter value 'n' at different time range 0-5 minutes and 5-60 minutes of annealing of $WSi_x/Si$ thin films at 1000°C

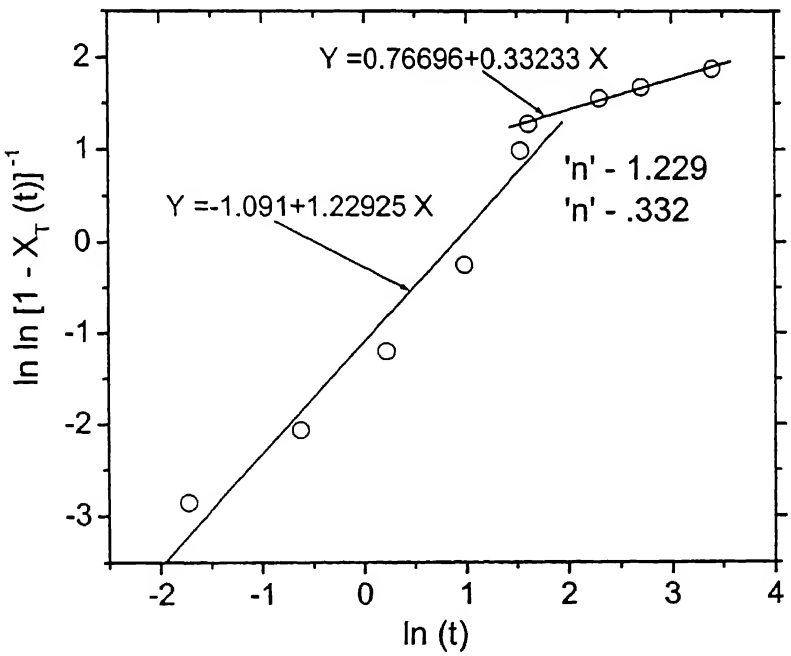


Fig 6.2 Fitting curve shows the growth parameter value 'n' at different time range 0-5 minutes and 5-60 minutes of annealing of $WSi_x/SiO_2/Si$ thin films at 1000°C

## 6.3 CONCLUSION

It is concluded from the above discussion that, the kinetics of phase transformation for $WSi_{2.4}$/Si and $WSi_{2.4}$/$SiO_2$ is based on diffusion controlled. Using the resistivity, as a measure of degree of crystallization, there does not seem to be and significant difference in the kinetics on two substrates. But evidence in chapter 5 points to differences in two cases, we think this could be due to the fact that resistivity is not a good measure of degree of crystallization. If the $WSi_2$ grains are interconnected, further grain growth will not change the resistivity significantly.

# CHAPTER 7

## CONCLUSIONS AND FUTURE PLAN

In this thesis, as-deposited and annealed tungsten silicide ($WSi_x$) films deposited on Si and $SiO_2$ substrate by chemical vapour deposition (CVD), have been studied by different characterization techniques in order to investigate the kinetics of phase transformation on both the substrates. The conclusions of the current study are given below:

### 7.1 AS-DEPOSITED FILMS

As-deposited films on Si and $SiO_2$ substrate are amorphous in nature. A uniform composition, Si/W ratio of 2.4 is obtained in both the film as reported by RBS studies. As-deposited resistivities are 15.2 ± $0.42\times10^{-4}$ Ω-cm and 14.1 ±$0.45\times10^{-4}$ Ω-cm for films deposited on Si and $SiO_2$ substrates, respectively. Thickness of $WSi_{2.4}$ films deposited on Si and $SiO_2$ are 5000 ±100Å and 4650 ±100Å, respectively.

### 7.2 ANNEALED $WSi_x$ FILMS

1. Based on resistivity, X-ray intensity and grain size measurement, it is concluded that 60 min annealing at 1000°C is not sufficient to completely crystallize the $WSi_x$/Si films. On the other hand, for annealing at higher temperature, at about 1100°C for 30 min, the decrease in resistivity as well as increase of grain growth ceases. It is inferred that going at higher temperature should be avoided by longer time of annealing at 1000°C to transform $WSi_{2.4}$ to $WSi_2$.
2. For $WSi_{2.4}/SiO_2$/Si films, the standard anneal process 30 minutes of anneal at 1000°C, seems to achieve complete crystallization and minimum resistivity possible.
3. Cross-sectional TEM shows evidence of random nucleation and deposition of excess Si at the interface. This is in agreement with our hypothesis that diffusion of excess Si in case of $WSi_x$/Si allows grain growth beyond the initial crystallization of first 5 minutes.

## 7.3 KINETICS OF PHASE TRANSFORMATION

1. Avarami model is used to investigate the phase transformation kinetics using resistivity data for calculating degree of crystallization. On $WSi_x/Si$, mode parameter "n" is 1.36 for first 5 min and 0.34 beyond that. This indicates random nucleation and parabolic growth for first five minutes. Beyond 5 min, there is saturation of nucleation sites and only grain growth is occurring. We find similar values for analysis on $WSi_x/SiO_2/Si$.
2. The kinetics model is consistent with RBS and TEM studies.

## 7.4 FUTURE PLAN

A more extensive interface study of cross-sectional TEM samples annealed at higher temperatures and time with varying Si/W ratio and thickness of the film will elucidate the kinetics of phase transformation. A more detailed study of kinetics of phase transformation can also be done by studying the relative effects of various parameters (listed above) on the annealing behaviour. This will lead the path for developing kinetics model that can predict the final film property if all the parameters are defined.

# REFERENCES


1. J.R Belch, "Etch Pit Formation in Si and Al-Si Contacts", J.Electrochem.Scociety 115, C 242 (1968)
2. S.P Muraka, "Refractory Silicides for Integrated Circuits", J.Vacum Science Technology, Vol 17, No.4, page 775 (1980)
3. F Mohammadi, K.C Saraswat, "Properties of Sputtered Tungsten Silicide for MOS Integrated Circuit Applications". J.Electrochem.Society, Solid State Science and Technology, Vol 127, No 2, page 450 (1980)
4. Y.Shioya, K.Ikegami, I.Kobayshi and M.Maeda, "Properties of Chemical Deposited Tungsten Silicide Films Using Reaction of $WF_6$ and $Si_2H_6$," J.Electochem.Sco. Solid -State Science and Technology, Vol 134, No 5, page 1220 (1987).
5. J.M Shaw and J.A Amic, "Vapor-deposited Tungsten as a Metallization and Interconnection Materials for Silicon Devices," RCA Review, June (1970).
6. L.D Locker and C.D Capio, "Reaction Kinetics of Tungsten Thin Films on a Silicon (100) Surface," J.Appl.physics, Vol 44, no 10, page 4366 (1973).
7. B.L Crowder and S Zirinsky, "1μm MOSFET VLSI Technology: Part VII-Metal Silicides Interconnection Technology-A Future Perspective," IEEE Trans.on Electron Devices, Vol.ED-26, no.4, page 369 (1979).
8. T.P Chow, D.H Bower, R.L Van art and W.Kantz, "Properties of Sputtered Silicide Thin Films", J.Electochem.Sco" , Vol 130, page 952 (1983).
9. F.Mohammadi and K.C Saraswat, "Properties of Sputtered Tungsten Silicide for MOS Integrated Circuit Application," J.Electrochem Sco, .Vol 127, page 454 (1980)
10. D.L Borors, J.A Monning and K.C Saraswat, "Properties of LPCVD Tungsten Silicide as Related to IC Process Requirements," Solid state Technology, Vol 26, page 183 (1983)
11. J.Rouse, F.Mohammadi, C.R Helms and K.C Saraswat, "App. Physics Letter", Vol 37, page 305 (1980)

12. F.M d'Heurle, C Dell'Oca and W.M Bullis Eds, "The Electrochem.Sco," page 194 (1982)
13. A.K Shinha, W.S Linden Berger, D.B Fraser, S.P Muraka and E.N Fuls, " IEEE Trans.Electron Devices, Vol ED-27, page 1425 (1980)
14. S.P Muraka, D.B Fraser, A.K Shinha and H.J Levin stein, IEEE Trans.Electron Devices, Vol.ED 27, page 1409 (1980)
15. H.Gielpel, Jr.N.Hsich, N.H Ishaq, C.W Koburger and F.R White, IEEE Trans.Electron Devices, Vol ED-27, page 1417 (1980)
16. K.C Saraswat, D.L.Brors, J.A.Fair, K.A.Monnig, and R.Beyers, "Properties of Low-Pressure CVD Tungsten Silicide for MOS VLSI Interconnections," IEE Transactions of Electron Devices, Vol.ED-30, No11 (1983)
17. F.M d' Heurle, C.S Peterson, and M.Y Tsai, "Observation On The Hexagonal Form of $MOSi_2$ and $WSi_2$ Films Produced by Ion Implantation and On Related Snowplough Effects," J.Appl.Phys, Vol 51, page 5976 (1980)
18. T.H Tom Wu, R.S Roseler, B.C.Lamartine, R.B.Gregory and H.G.Tompkins, "Properties of $WSi_x$ Using Dichlorosilane in a Single- Wafer System," J.Vac Sci.Technology B, Vol 6, N.O 6 (1988)
19. M.Y Tsai, F.M. d Heurle, C.S Peterson, and R.W Johnson, "Properties of Tungsten Silicide Film on Polycrystalline Silicon," J.Appl.Phys.Volume 52, no 8, page 5350 (1981)
20. F.Nava, B.Z Weiss, K.H Ahn, D.A smith and K.N Tu, " Thermal Stability and Electrical Conduction Behaviour of Co-evaporated $WSi_{2\pm x}$ Thin Films", J.Appl.Phys.64, Vol1, page 354 (1988)
21. Y.Shioya and M.Maeda, "Analysis of The Effects of Annealing on Resistivity of Chemical Vapour Deposition Tungsten-Silicide Films," J.Appl.phys, Volume 60, No 1, page 327 (1986)
22. T.Hara, T.Miyamoto, H Hagiwara, E.I Bromley ad W.R Harsh Barger, "Composition of Tungsten Silicide Films deposited by Dichlorosilane Reduction of Tungsten Hexafluoride," J Electrochem.Soc, Vol 137, No.9, page 2955 (1990)

23. S.G Telford, M.Eizenberg, M.Chang, A.K Sinha and T.R Gow, "Formation of Compositionally Uniform Tungsten Silicide Films Using Dichlorosilane in a Singe-Wafer Reactor," Appl.Physics Letter, Volume 62, no15, page1766 (1993)
24. J.S.Byun, B.H.Lee, J.Park, D.Sohn, S.J.Choi and J.J Kim, "Formation of High Conductivity $WSi_x$ Layer and Its Characterization as a Gate Electrode. J.Electrochem.soc, Vol.145, No.9, page 3228 (1998)
25. M.Katiyar, G.S Samal, R.K Gupta, P.K sahoo[1], V.N Kulkarni[1], O.Adetutu[2] "Substrate Dependence of The Annealing Behaviour of $WSi_{2\,4}$ Films Prepared by CVD" J.Applied Physics Letters.
26. J.H Liang, D.S Chao " Formation of Tungsten Silicide Films by Ion Beam Synthesis" Vol.140, No 2, page 116 (2001)
27. D.K.Schroder, "Semiconductor Materials and device Characterizations," Edition by John Wiley 2-15 (1990)
28. W.K.Chu, J.M Mayer, and M.A Niclot, "Rutherford backscattering Spectroscopy" (Academic press), New York, (1978)
29. "Phase Transformation Kinetics During Thermal Annealing of Tungsten Silicide Films", A thesis by "Girija Shankar Samal"(1999)
30. J.C.Bravman and R.Sinclair, J.Electron.Micros.Tech. Volume1, page 53 (1984)
31. D.F Dawson-Elli, M.A Turowski, T.F Kelly, Y.W Kim, N.A Zreiba, T.C.Ming and Z.Mei, Mater Res.Sco.proc. 199, page 137 (1990)
32. V.E Borisenko (Ed.) "Semi conducting Silicides", Springer series in materials science.
33. S.O.Hyatt, D.O.Northwood: "A thermodynamic aspect to the sequence of phase formation in thin films; Application to Ti, V, Cr, and Mn with Si", Mater.forum volume17, No.3, page 251 (1994)
34. R.Pretorious, C.C.Theron, A.Vantomme, J.W.Mayer, "Compound Phase Formation in Thin Film Structures", Critical Reviews in Solid State and Materials Science, Volume 24, No.1, page 1-62 (1999)
35. R.C Sharma, "Phase Transformation in Materials" CBS Publishers ( Delhi) (2002), ISBN 81-239-0794-X

36. A.Hiraki, "Metal-Semiconductor Interfaces", IOS Press, Japan (1995), ISBN 90-5199-205-X
37. K.Morigaki, "Physics of Amorphous Semiconductors", Imperial College Press, London (1999), ISBN 981-02-1381-6
38. A.G Cullis and D.B.Holt " Microscopy of Semi conducting Materials, 1985 Proceedings of the Royal Microscopical Society Conference Held in St Catherine's College, Oxford, 25-27 March 1985, , ISBN 0-85498-167-5
39. M.F Bain, B.M Armstrong and H.S Gamble "The Deposition and Characterization of CVD Tungsten Silicide for Applications in Microelectronics" 17 December 2001
40. J.A Kittal, D.A Prinslow, P.P Apte and M.F Pas "Kinetics and Nucleation Model Of The C49 to C54 Phase Transformation in $TiSi_2$ Thin Films on Deep- Sub-Micron Type Polycrystalline Silicon Lines" Appl.Phys.Letter, no.67 (16), Page 2308 (1995)